THESIS FOR THE DEGREE OF DOCTOR OF PHILOSOPHY

Key Aspects of Sintering Powder Metallurgy Steel Prealloyed with Chromium and Manganese

OLA BERGMAN

Department of Materials and Manufacturing Technology
CHALMERS UNIVERSITY OF TECHNOLOGY
Gothenburg, Sweden 2011

Key Aspects of Sintering Powder Metallurgy Steel Prealloyed with Chromium and Manganese
OLA BERGMAN
ISBN 978-91-7385-577-8

Doktorsavhandlingar vid Chalmers tekniska högskola
Ny serie nr 3258
ISSN 0346-718X

Department of Materials and Manufacturing Technology
Chalmers University of Technology
SE-412 96 Gothenburg
Sweden
Telephone + 46 (0)31-772 1000

Printed by Chalmers Reproservice
Gothenburg, Sweden 2011

Key Aspects of Sintering Powder Metallurgy Steel Prealloyed with Chromium and Manganese

OLA BERGMAN

Abstract

The powder metallurgy (PM) process is a cost efficient near net-shape technology suitable for sustainable manufacturing of structural steel components. A drawback with the PM technology is the difficulty to use oxidation sensitive alloying elements, such as Cr and Mn. These are effective alloying elements and their cost is significantly lower than the cost of the most commonly used alloying elements (Cu, Ni and Mo) in PM steel. Hence, increased usage of Cr and Mn as alloying elements in PM steel is crucial for retaining the competitiveness of the PM technology versus other metal forming processes. Sintering is the most critical process step when manufacturing PM steel parts from oxidation sensitive powder. The research work presented in this thesis was aimed at building a fundamental knowledge platform regarding key aspects of sintering PM steel prealloyed with Cr and Mn. These aspects are sintering atmosphere requirements, oxide reduction mechanisms, and effects of residual oxides on mechanical properties of the sintered material.

The test materials used in the research studies were four different water-atomized steel powder grades prealloyed with 3%Cr-0.5%Mo, 1.5%Cr-0.2%Mo, 1.8%Cr and 0.8%Cr-0.4%Mn. Compacted specimens based on these powder grades were used for sintering experiments in N_2/H_2 (90/10) atmosphere at temperatures in the range of 1120-1300°C. Oxide reduction reactions during sintering were studied by the means of photoacoustic spectroscopy. Mechanical properties of the sintered specimens were evaluated through hardness measurements, tensile tests and impact tests. The analysis techniques used for evaluation of specimen microstructures and fracture surfaces were light-optical microscopy and scanning electron microscopy combined with energy dispersive X-ray spectroscopy.

The research work shows that the critical oxygen partial pressure in the sintering atmosphere can be well-predicted by thermodynamic calculations of oxide stabilities in the steel. Stable Cr-Mn spinel oxides on the powder surfaces are reduced via carbothermal reactions at temperatures above 1000°C. Sintering for 30 minutes at 1120°C in a reducing atmosphere gives incomplete reduction of these oxides, which does not affect the sinter neck formation in the PM part. Increased sintering temperature to 1200-1250°C enables nearly complete oxide reduction, although high PM part density may obstruct the reduction of the stable oxides due to less effective CO diffusion in the pore system of the part. Residual oxides after sintering are in the form of micrometer size particulate features and these have no detrimental effect on the evaluated mechanical properties of the PM steel.

Keywords: Powder metallurgy, PM steel, Chromium, Manganese, Prealloyed, Sintering, Atmosphere, Oxide reduction, Spinel oxide, Residual oxides, Mechanical properties

Preface

The research work presented in this thesis was carried out at the Swedish Institute for Metals Research (today Swerea KIMAB AB) in the years 1999-2001 and at Höganäs AB from year 2001 until present date. During the years 2008-2010, the research studies were conducted in close collaboration with the Department of Materials and Manufacturing Technology at Chalmers University of Technology. The thesis consists of an introductory part and the following appended papers:

I. **Influence of Oxygen Partial Pressure in Sintering Atmosphere on Properties of Cr-Mo Prealloyed Powder Metallurgy Steel**
O. Bergman
Powder Metallurgy, 2007, Vol. 50, No. 3, pp. 243-249.

II. **Influence of Sintering Parameters on the Mechanical Performance of PM Steels Prealloyed with Chromium**
O. Bergman, B. Lindqvist and S. Bengtsson
Materials Science Forum, 2007, Vols. 534-536, pp. 545-548.

III. **Analysis of Oxide Reduction during Sintering of Cr-alloyed Steel Powder through Photoacoustic Spectroscopy Measurements**
O. Bergman, K. Frisk and L. Nyborg
Proc. of Euro PM2009, Copenhagen, Denmark, Oct. 2009, EPMA, Vol. 3, pp. 239-244.

IV. **Evaluation of Sintered Properties of PM Steels based on Cr and Cr-Mn Prealloyed Steel Powders**
O. Bergman and L. Nyborg
Powder Metallurgy Progress, 2010, Vol. 10, No. 1, pp. 1-19.

V. **Study of Oxide Reduction Mechanisms during Sintering of Powder Metallurgy Steel based on Water-Atomized Steel Powder Prealloyed with Cr**
O. Bergman and L. Nyborg
Submitted to Metallurgical and Materials Transactions A, August 2011.

Contribution to the Appended Papers

The contribution by the author to the research work presented in the appended papers consists of all thermodynamic calculations, the sintering trials and metallography for Paper I, the fractography for Paper IV and part of the metallography for Paper V. The original manuscripts for all papers have been written by the author and the finalization of the manuscripts has been done in collaboration with the co-authors. A summary of the contribution by others to the performed research studies follows below.

Paper I: Mechanical testing, chemical analyses and density measurements were performed by laboratory technicians at Höganäs AB.

Paper II: Sintering trials and all evaluation of material properties were performed by laboratory technicians at Höganäs AB. The microstructure analysis was done by the Metallography Department at Höganäs AB.

Paper III: Sintering trials were performed by Swerea KIMAB AB. Chemical analyses and density measurements were done by laboratory technicians and microstructure analysis was done by the Metallography Department at Höganäs AB.

Paper IV: Sintering trials and all evaluation of material properties were performed by laboratory technicians at Höganäs AB. The microstructure analysis was done by the Metallography Department at Höganäs AB. Eduard Hrhya at Chalmers University of Technology assisted during the fractography evaluation.

Paper V: Sintering trials were performed by Swerea KIMAB AB. Chemical analyses and density measurements were done by laboratory technicians and part of the microstructure analysis was done by the Metallography Department at Höganäs AB.

Contents

1. Introduction

Powder metallurgy (PM) is a near net-shape technology which is commonly applied in the production of structural steel components. The PM process involves pressing powder into a compact of defined shape and subsequent heating, or *sintering*, the compact so that the powder particles bond together. The shape of the compact after pressing is close to the shape of the final component and the dimensional change of the compact during sintering is relatively small. Therefore, the need for machining or other sizing operations after sintering is usually limited. The near net-shape feature of the technology and the few process steps needed make the PM process very competitive towards other technologies in the production of structural steel parts. The main advantages compared to conventional metal forming processes (forging, casting, machining, etc.) are high material utilization, low energy consumption and short overall production time [1]. These advantages mean that the manufacturing cost generally is much lower for a PM component than for corresponding component produced by e.g. machining from stock bar, especially in the case of large series of a component with complex shape. Another advantage of using the PM process is that materials with unique compositions and microstructures can be produced due to the possibility of mixing different types of powder. Furthermore, the energy efficiency and the high material-utilization factor of the process mean that PM is a recognized "green" technology for sustainable manufacturing [2].

A drawback with the PM technology is that components produced by the conventional press-sinter route do not obtain full density. The PM parts typically have around 10% porosity, with the implication that the mechanical performance is lower compared to fully dense steel parts. Consequently, the most highly loaded structural components are difficult to produce by means of the PM process route. Another limitation of the PM technology has been the difficulty to use oxidation sensitive alloying elements, such as chromium and manganese. Both Cr and Mn are commonly used in conventional low-alloy steel, since they are effective alloying elements and low cost metals. In PM steels, on the other hand, alloying with Cr and Mn has for many years been very limited. The reason for this is that these elements have high affinity for oxygen and strong tendency to form stable oxides, which makes oxidation and oxide reduction during PM processing challenging issues. Instead, the more processing friendly metals copper, nickel and molybdenum are the most commonly used alloying elements in PM steels. However, these metals are relatively expensive and in recent years the prices of Mo and Ni have been volatile and reached very high levels, as illustrated in Figure 1. Comparison of the monthly prices of the different metals in the years 2006-2010 shows that the price of Cr in average has been 20% of the price of Ni and only 9% of the price of Mo during this period, and the Mn price has constantly been even lower than the Cr price. There are also other reasons for replacing existing alloying elements with Cr and Mn, such as the recycling problems associated with Cu and the health hazards of handling Ni. Consequently, increased usage of Cr and Mn as alloying elements in PM steel grades is crucial for maintaining and strengthening the competitiveness of the PM technology in the production of structural steel components.

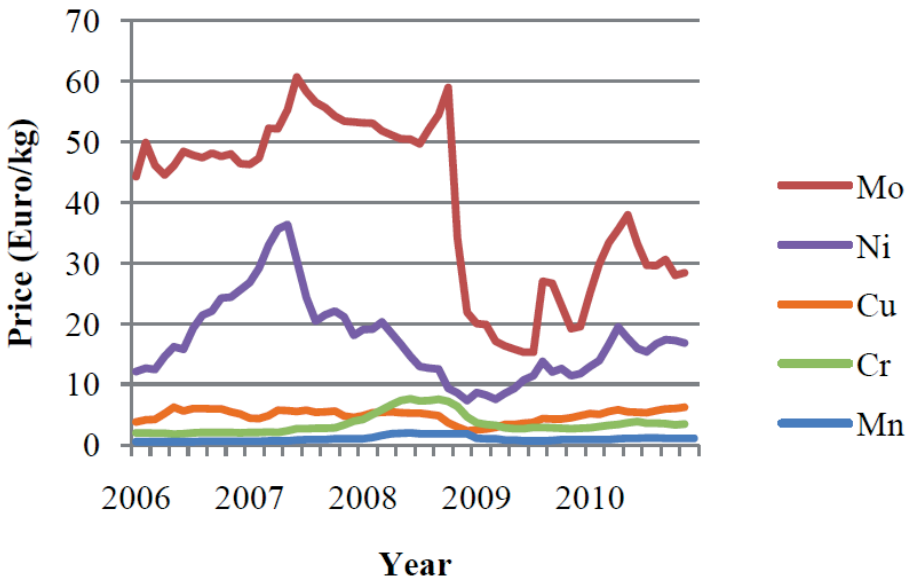

Figure 1. Metal prices during the years 2006-2010 (source: London Metal Exchange).

Employment of oxidation sensitive alloying elements in PM steel grades means that special requirements are put on both the powder manufacturing process and the process route for PM component production. The powders are manufactured through water-atomization, which inevitably leads to formation of oxide layers on the powder surfaces. The presence of strong oxide formers, such as Cr and Mn, in the steel alloy give surface oxides that are relatively difficult to reduce in the subsequent powder annealing process. Therefore, the manufacturing of powder containing these alloying elements has historically been hard to accomplish in a cost efficient way. However, process development efforts in recent years have changed the situation and about a decade ago two Cr-alloyed powder grades were introduced on the market [3, 4]. These grades are today well-established as cost-effective materials suitable for production of high-performance PM steel parts. Still, insufficient knowledge regarding how to successfully process the powders into components has been limiting the application of the Cr-alloyed materials.

Sintering is the most critical process step when it comes to manufacturing of PM steel components from oxidation sensitive powder grades. A high-purity protective atmosphere is required to prevent oxidation of the materials in the process. Furthermore, the applied temperature cycle has to provide sufficient reduction of thermodynamically stable oxides on the powder surfaces to secure that efficient bonding between powder particles occurs. The research work presented in this thesis has been aimed at building up a fundamental knowledge platform regarding sintering of powder grades prealloyed with Cr and Mn, with emphasis on *sintering atmosphere requirements*, *oxide reduction mechanisms*, and *effects of residual oxides on mechanical properties* of the sintered material. The knowledge platform constitutes an essential part in the work towards increased usage of Cr and Mn as alloying elements in PM steel grades.

2. Powder Metallurgy

2.1 Brief history

The origins of PM can be traced back several thousand years in time, since it is known that Egyptians heated iron ore to produce metallic iron powder around 3000 BC [5]. They used this iron powder to make tools by hammering to weld powder particles together at elevated temperatures. The inability at that time to melt iron was the driving force for developing the PM process. In more modern times, PM was first used in large scale in Europe and Russia during the 1800s to produce platinum laboratory crucibles. The next big step for PM was when Coolidge used tungsten powder to develop filaments for electric light bulbs in 1910. Around the same time, industrial production of PM molybdenum articles for the electrical industries also started. Several important PM products were developed in the 1920-1930s, such as cemented carbides (WC-Co) for cutting tools and porous self-lubricating bearings for small rotating or reciprocating machinery.

After the Second World War, iron based PM structural parts were developed on a commercial scale. These PM steel parts were developed as lower cost alternatives to components produced by the traditional processes casting, forging, stamping, and machining from stock bar. Since then there has been a steady increase in the production of PM structural steel parts, especially in the last few decades, and the mass production of PM steel components is today the most significant use of the PM technology.

2.2 Iron and steel powder production

Practically all iron and steel powder for PM steel components is produced by either of two different production processes, a *solid state reduction process* (also known as the Höganäs sponge iron process) or a *water-atomization process* [6].

In the reduction process, finely divided highly pure iron ore (Fe_3O_4) and a reduction mix consisting of coke and limestone are used as starting materials. These materials are heated to a temperature of around 1200°C. When the coke is heated, CO forms and reacts with the iron ore to reduce it to metallic iron, while the limestone binds the sulphur contained in the coke. The iron particles sinter together and form porous iron sponge. After the reduction process, the iron sponge is cleaned, crushed and milled into crude powder. Subsequently, the powder is soft-annealed at 800-900°C whereupon the remaining carbon and oxygen contents are reduced to very low levels. Finally, the lightly sintered powder cake is milled and sieved to a press-ready so called *iron sponge powder* with highly irregular shape suitable for the press-sinter process route.

In the water-atomization process, carefully selected iron scrap and sponge iron from the reduction process are melted in an electric arc furnace. Alloying metals may also be added to the melt. After refining of the melt, the liquid metal is emptied from a tundish in a well-controlled stream through a nozzle, where high pressure water jets hit the stream and divides it into droplets that solidify into powder particles (see Figure 2). The obtained particles are hard (martensitic) and covered by *surface oxides*, due to the very high cooling rates and the water vapour present during atomization. Therefore, the powder is annealed in order to soften the material and to reduce surface oxides. Most of the surface oxides are reduced in this process, but there are still thin layers of oxides on the powder surfaces after annealing. Different annealing temperatures are used for different alloys. Annealing is followed by milling and sieving to a press-ready powder. As for the sponge powder, also the *water-atomized powder* has a highly irregular shape suitable for the press-sinter process route (see Figure 3). Water-atomized powders have generally lower impurity levels and are more compressible than sponge powders. Powder for pressing and sintering typically has a normal particle size distribution with mean particle size of around 70-80 μm. In between 10% and 30% of the powder particles are usually below 45 μm in size while less than 10% of the particles are above 150 μm in size.

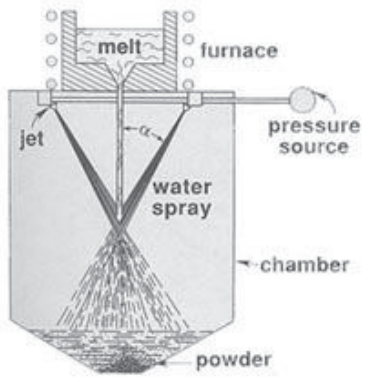

Figure 2. Illustration of water-atomization process (re-printed from [1]).

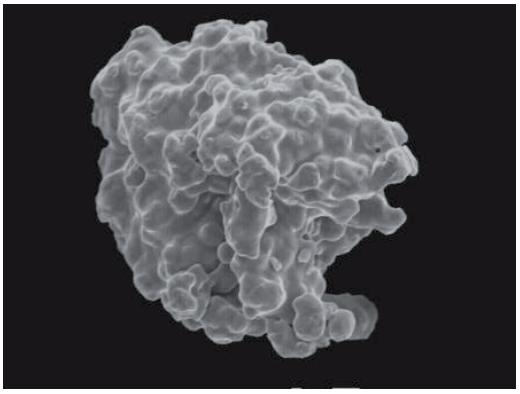

Figure 3. High magnification of powder particle (size ~75 μm) produced by water-atomization and subsequent annealing.

2.3 Alloying elements and alloying methods

The most commonly used alloying elements (besides carbon) in low-alloy PM steel are copper, molybdenum and nickel. These elements are not strong oxide formers and are therefore suitable to use in the manufacturing of powder and PM components. Elemental Cu is widely used as additive in powder mixes, since Cu melts during sintering and acts as sintering activator. However, the hardenability effect of Cu is relatively low compared to other alloying elements. Molybdenum has high hardenability effect and is a strong carbide forming element. It is also beneficial for the material strength at elevated temperatures.

Nickel improves the strength and toughness of the steel, but provides lower hardenability than Mo. The austenite stabilizing effect of Ni may lead to retained austenite in the material structure at high carbon content.

Chromium and manganese are effective alloying elements in low-alloy steel but their oxidation sensitivity makes them challenging to process via the PM route. Chromium is today used in relatively large scale in PM steel alloys, while the use of Mn is still very limited. The alloying effect of Cr is similar to that of Mo, i.e. high hardenability effect is provided and the material strength at elevated temperatures is improved. Chromium is also a carbide forming element, which can be utilized to obtain good wear resistance. Manganese has a significant effect on the hardenability of steel. Another beneficial effect of alloying with Mn is that it counteracts brittleness from sulphur through the formation of Mn sulphides.

There are basically three different methods used to introduce alloying elements in PM steel:

- Pre-mixing
- Diffusion-alloying
- Pre-alloying

Pre-mixing means that iron powder is mixed with alloying elements in powder form before the pressing operation. During the subsequent sintering, alloying occurs through diffusion processes. The main advantage with pre-mixing is that pure iron powder has high compressibility. Disadvantages are that the sintered parts obtain inhomogeneous compositions due to slow diffusion of alloying elements (except carbon), and that the alloying element particles tend to segregate during handling and transportation of the powder mixes. Carbon is generally added by pre-mixing with graphite. It is also common to alloy with copper by means of pre-mixing.

Diffusion-alloying is a method to bond fine alloying element particles (typical size 10 μm) onto the surfaces of iron powder. This is done through an annealing process where the bonding between particles is caused by diffusion. Hereby, segregation of alloying element particles is minimised while the high compressibility is retained. However, sintered parts made from diffusion-alloyed powder will still have inhomogeneous composition. Diffusion-alloyed powder is made from both sponge powder and atomised powder. Alloying elements used in diffusion-alloyed powder are generally Ni, Mo and Cu.

Pre-alloying means that the alloying elements are added to the melt before the water-atomization, which results in homogeneously alloyed powder particles. Consequently, sintered parts made from prealloyed powder will have homogeneous compositions and segregation problems in powder mixes are not an issue. The downside with pre-alloying is that the powder is less compressible than a pure iron powder due to solution-hardening effects. Molybdenum is commonly used in prealloyed powder grades, since Mo has

relatively small effect on the compressibility. Steel powder prealloyed with Mo is also used as base in some diffusion-alloyed powder grades. Furthermore, the pre-alloying method opens up for introduction of oxidation sensitive alloying elements, such as Cr and Mn, which are difficult to introduce by means of the other alloying methods.

2.4 Manufacturing of PM steel components

The process route for manufacturing of PM steel components is presented in Figure 4. The main process stages are *mixing*, *compaction* (pressing) and *sintering*. These stages are described below with special emphasis on sintering, which is the key process in the context of this thesis. *Secondary operations* such as sizing, machining or different heat treatments (e.g. case hardening, through hardening) may be applied after sintering in order to improve tolerances and mechanical properties of the components. These operations are not treated further here.

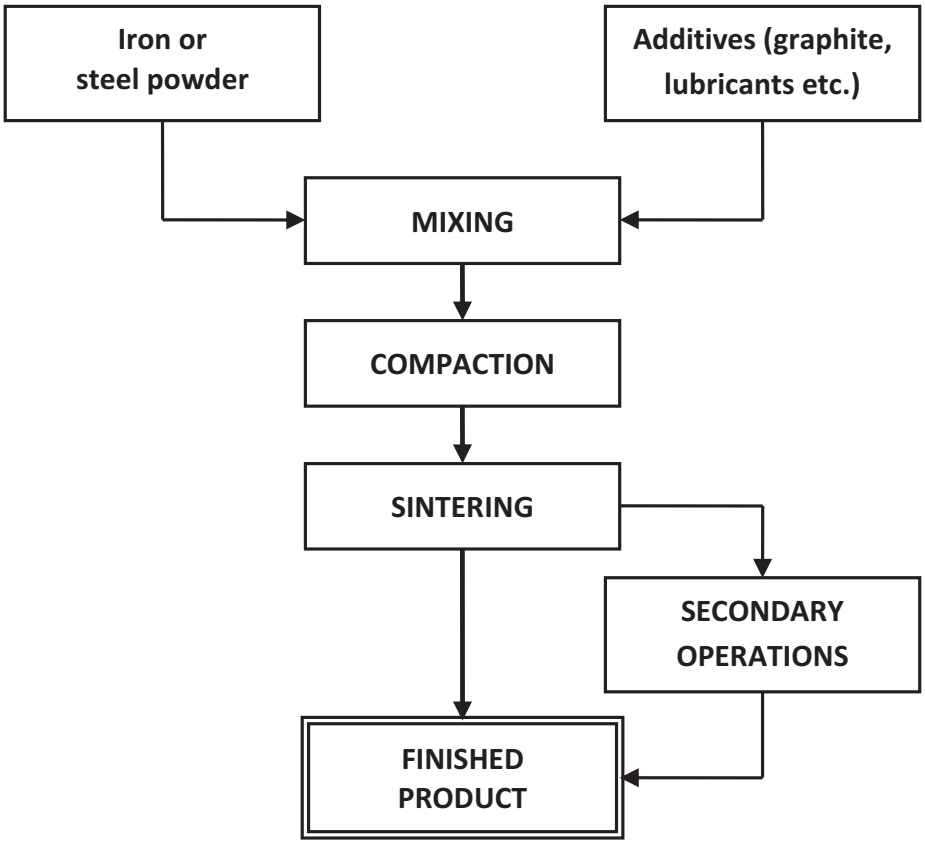

Figure 4. Schematic overview of the process route for manufacturing of PM steel components (author's illustration).

Mixing

Iron or steel powder is generally mixed with graphite powder and, optionally, other alloying additive particles (e.g. Cu). An organic substance (lubricant powder) is normally added in order to have lubrication during the compaction step. Other additives may also be admixed as, for example, substances that facilitate machining of sintered components. Particle sizes of graphite, lubricant and additive powders are usually small, typically below 10 μm. Some alloying additives have larger particle sizes. The mixing process may also involve special treatments of the powder mix, where certain types of organic binders are used to glue graphite, lubricants and other additives to the iron/steel powder. Such a process improves product consistency and minimizes problems with segregation and dusting.

Compaction

The compaction process starts with the filling of a powder mix into the cavity of a (usually rigid) die. In the die, the powder mix is compacted between two or more axially moving upper and lower punches to form a porous compact of more or less complicated shape. Finally, the obtained compact is pushed out from the die by the lower punches. During compaction, the powder particle surfaces are smoothed, oxide skins are broken, particles are deformed and cold-welding occurs between particles. The irregular shape of the powder gives efficient cold-welding and interlocking between the particles. Hereby, the powder compact acquires sufficient strength to allow handling before the sintering operation. Lubrication between die wall and powder mass is important during compaction as well as ejection. Hence, the need for lubricant additions in the powder mixes is evident.

There are limitations in the compact densities that can be achieved by the conventional die compaction process, mainly due to practical restrictions in compaction pressure and presence of the lubricant in the powder mix. One method to reach higher densities is to heat the powder and the die (normally to about 150°C) prior to compaction combined with the use of a specially designed polymer as lubricant. The application of this process, called *warm compaction* (WC), gives higher and more even component densities than conventional compaction at room temperature [7]. A modified version of the warm compaction process is *warm die compaction*, where only the die is heated and not the powder [8]. Another method is to use *high velocity compaction* (HVC) by which the density can be raised typically 0.3 g/cm^3 compared to conventional compaction [9]. There is also the *double press – double sintering* (2P2S) technique, where a second compaction step is applied after pre-sintering of the components, as well as *powder forging* (PF), where full density is achieved through forging of a pressed and sintered preform. However, the application of these techniques lead to higher production costs and conventional *cold compaction* (CC) is therefore the most frequently used forming technique in mass production of PM steel parts.

Sintering

In the sintering process, the compacted green bodies are heated to high temperature in order to obtain bonding between the powder particles. This bonding occurs through the formation of *sinter necks* between particles that are in contact with one another after the compaction. The sinter neck formation, which provides mechanical strength to the PM steel components, is driven by the minimization of surface energy and progresses through atomic diffusion processes [10]. A prerequisite for efficient sinter neck formation is that surface oxides on the powder particles are sufficiently reduced in the early stages of the sintering process [11-13]. Oxide reduction during sintering is treated further in chapter 4.

A typical sintering process cycle consists of a *heating-up phase*, during which the organic lubricant burns off (*de-waxing*) from the compacts, a *sintering phase*, where the parts are held at constant temperature for enough time to achieve sufficient bonding between metal particles, and finally a *cooling phase*, in which the microstructure of the steel is decided by the cooling rate. The sintering cycle is illustrated in Figure 5.

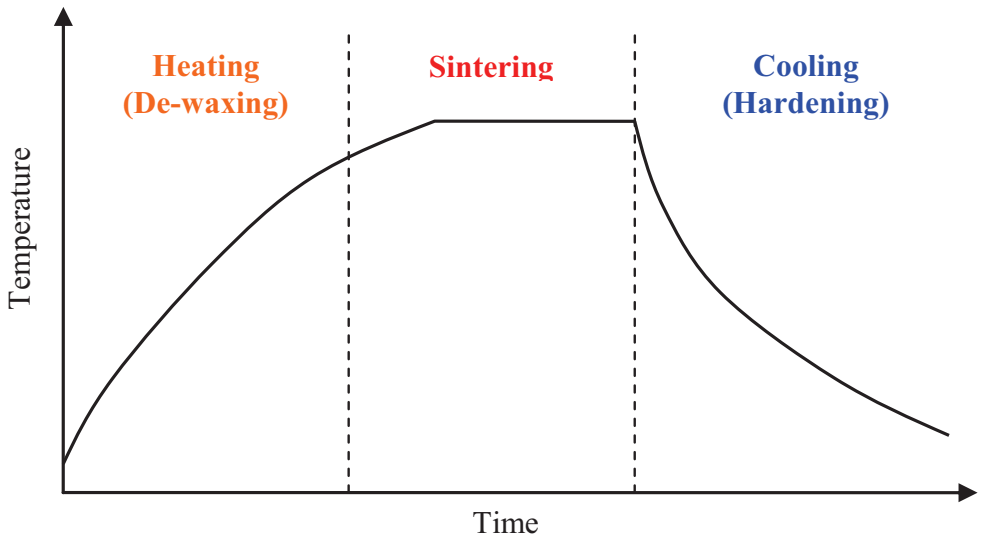

Figure 5. Typical temperature-time profile for PM steel parts during sintering (author's illustration).

Continuous sintering furnaces are most often used for the production of PM steel parts, mainly due to their high productivity. These furnaces usually have wire mesh belts on which the parts are conveyed through different zones or chambers for de-waxing, sintering and cooling. The de-waxing zone may be equipped with a rapid burn-off unit, to ensure fast and efficient lubricant removal. Moreover, some furnaces have fans in the cooling zone so that accelerated cooling can be applied in order to harden the steel components, so called *sinter hardening*.

Mesh belt furnaces are used at temperatures of up to 1150°C and the upper temperature limit is decided by heat resistance of the belt material [14]. A typical sintering temperature in industrial production is 1120°C and the time at temperature is usually in the range of 15-30 minutes. There are other types of sintering furnaces for higher sintering temperatures. For example, walking beam furnaces and continuous pusher furnaces can be used at temperatures of up to 1350°C with relatively high production throughputs. Advantages with high temperature sintering are that oxides are more easily reduced due to higher thermodynamic driving force and that more efficient sinter neck formation is achieved due to faster diffusion processes. However, shrinkage of the PM parts increases at higher temperatures, which means that *dimensional control* during sintering becomes more difficult. Small dimensional change during sintering is generally demanded, since the final shape of the PM component usually is established already in the compaction process.

Protective gas atmospheres are used in the sintering furnaces and these play a very important role in sintering of PM steels. The main task of the sintering atmosphere is to prevent oxidation of the compacts during sintering and to participate in reduction of oxides remaining from the powder processing. Usually, the protective gas flows from the sintering zone into the de-waxing zone of the sintering furnace, thus preventing lubricant vapours from entering and ensuring that gaseous reaction products are transported out from the high-temperature zone. Most commonly used as protective atmosphere is so called *endogas*, which is produced through combustion of hydrocarbons and consist typically of ~40% H_2, ~20% CO, ~40% N_2, and small amounts of CO_2, CH_4, H_2O and O_2. Endogas atmospheres are dried to make them reducing during sintering of ferrous components. However, steels containing oxidation sensitive elements (e.g. Cr and Mn) require protective atmospheres with lower oxygen content. Such PM steel grades are therefore sintered in high purity N_2 atmospheres with up to 10% H_2 added for oxide reduction.

Monitoring of the oxygen content of a sintering atmosphere is usually done either directly through an oxygen sensor or indirectly through a *dew point* sensor. Dew point is the saturation temperature to which air must be cooled at constant pressure for water vapour to condense into water. Hence, the dew point is a measure of the H_2O content in the gas, from which the oxygen content can be calculated for an atmosphere with known H_2 content by considering the following equilibrium reaction:

$$H_2(g) + \frac{1}{2}O_2(g) \leftrightarrow H_2O(g) \qquad (1)$$

Another important task of the protective atmosphere is to prevent decarburization of the PM steel during sintering, particularly at the component surfaces. Therefore, the atmosphere should have a *carbon activity* which is equal to or slightly higher than the carbon activity in the steel. The carbon activity of the atmosphere can be calculated from the CO:CO_2 ratio in the gas by considering equilibrium reaction (2) [15]. In dry N_2-H_2 sintering atmospheres, where the CO content is too low to provide any significant carbon activity, it is common to use additions of low amount of CH_4 in order to prevent decarburization. For such atmospheres the carbon activity can be calculated from the

CH_4:H_2 ratio in the gas by considering equilibrium reaction (3) [15]. However, it is difficult to control the carbon activity in N_2-H_2-CH_4 atmospheres during sintering. Another approach is to use controlled additions of CO in N_2-H_2 sintering atmospheres. This approach provides the possibility to have good carbon control during sintering of oxidation sensitive PM steel grades, by continuous monitoring and steering of the CO and O_2 contents in the atmosphere [16, 17]. The carbon activity of the gas is in this case calculated from equilibrium reaction (4).

$$2CO(g) \leftrightarrow C(s) + CO_2(g) \quad (2)$$

$$CH_4(g) \leftrightarrow C(s) + 2H_2(g) \quad (3)$$

$$CO(g) \leftrightarrow C(s) + \frac{1}{2}O_2(g) \quad (4)$$

2.5 Mechanical properties of PM steel

The mechanical performance of PM steel is primarily decided by the *density* and the *microstructure* of the sintered parts. A schematic illustration of the influence of part density on different mechanical properties is presented in Figure 6. The figure shows that PM steel have considerably lower properties than fully dense steel at the densities (<7.15 g/cm^3) normally obtained in a conventional press-sinter process route. In particular elongation to fracture and impact strength properties of PM steel are generally low compared to those for corresponding steel with full density. These properties increase drastically with increasing part density from 7.0 g/cm^3 and above. Tensile strength and fatigue strength properties of PM steel increase roughly linearly with increasing part density throughout the density range 6.4-7.8 g/cm^3.

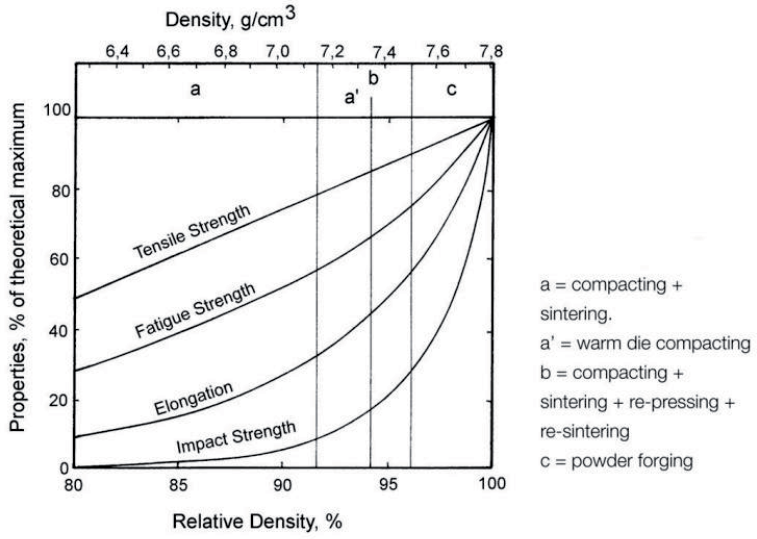

Figure 6. Schematic illustration of how mechanical properties of PM steel vary with density of the sintered part (re-printed from [18]).

The type of microstructure obtained in a PM steel part depends on the alloy composition of the material and the cooling rate applied after sintering. Materials based on pre-mixes (such as Fe-Cu-C mixes) and diffusion-alloyed steel powder generally have heterogeneous microstructures due to the relatively low diffusion rates of alloying elements (except carbon) during sintering. Diffusion-alloyed PM steel types typically contain mixtures of several different microstructure constituents (e.g. martensite, bainite, pearlite and Ni-rich austenite) and their mechanical properties are characterized by combinations of medium to high strength and relatively high ductility. Examples of typical as-sintered properties of two such steel grades, Distaloy AB (Fe-1.75%Ni-1.5%Cu-0.5%Mo) and Distaloy AE (Fe-4%Ni-1.5%Cu-0.5%Mo), are given in Table 1.

Table 1. Typical mechanical properties (at sintered density 7.1 g/cm^3) of different PM steel grades after sintering at 1120°C for 30 minutes and subsequent cooling with 0.5-1°C/s (2-3°C/s for Astaloy CrM). Data are taken from [18, 19].

Material	HV10	UTS (MPa)	YS (MPa)	A (%)	IE (J)
Distaloy AB + 0.6% C	205	620	450	2.8	20
Distaloy AE + 0.5% C	220	730	460	2.8	25
Astaloy Mo + 0.8% C	200	660	520	1.3	15
Astaloy CrL + 0.8%C	270	850	700	1.5	14
Astaloy CrM + 0.4% C	360	1100	950	0.5	14

HV10 = Vickers hardness, UTS = ultimate tensile strength, YS = yield strength, A = elongation to fracture, IE = impact energy

PM steel materials based on prealloyed steel powders generally have homogeneous microstructures since the alloying elements are evenly distributed in the powder grades from the start. A commonly applied prealloyed powder grade is Astaloy Mo (Fe-1.5%Mo) and PM parts produced from this grade (with 0.6-0.8% C added) obtain fully bainitic microstructures after sintering in a conventional belt furnace with subsequent cooling at 0.5-1.0°C/s [20]. Typical mechanical properties for this PM steel alloy (with 0.8% C added) are included in Table 1. A powder grade with similar total alloying content as Astaloy Mo is the Cr-Mo prealloyed material Astaloy CrL (Fe-1.5%Cr-0.2%Mo). The microstructures obtained in PM parts based on this grade (with 0.6-0.8% C added) consist of mixtures of bainite and fine pearlite after conventional sintering [21]. Hereby, higher mechanical performance is obtained compared to that of fully bainitic Astaloy Mo based PM steel, as the typical as-sintered properties in Table 1 demonstrate. Another Cr-Mo prealloyed powder grade is Astaloy CrM (Fe-3%Cr-0.5%Mo), which has excellent hardenability as illustrated by the CCT (Continuous Cooling Transformation) diagram in Figure 7. Fully martensitic microstructures are obtained in PM parts based on this powder grade (with addition of 0.4% C) when rapid cooling at rates above ~2°C/s is applied after sintering. Such PM parts have high hardness and strength as shown by the typical mechanical properties of sinter-hardened Astaloy CrM presented in Table 1.

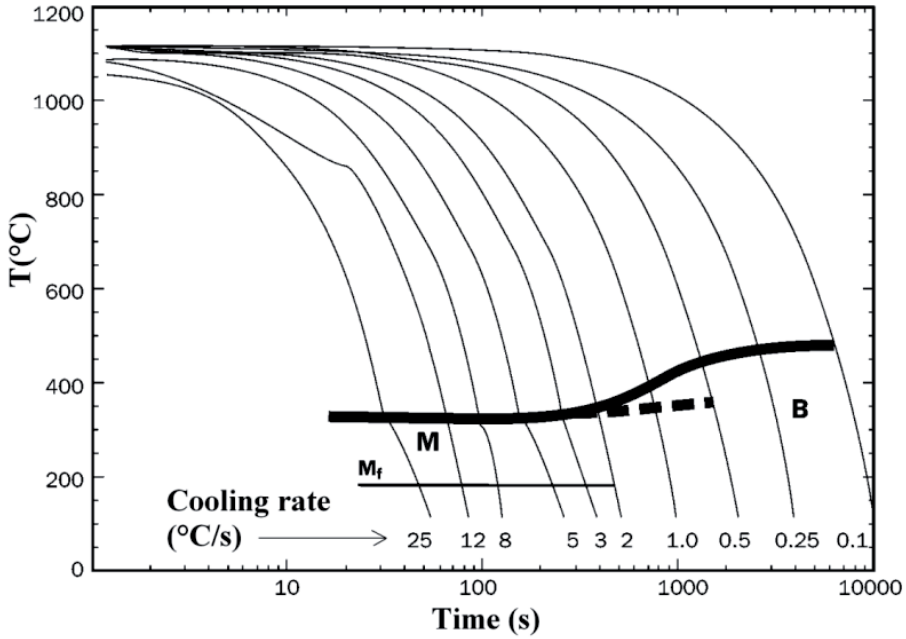

M = martensite, B = bainite

Figure 7. CCT diagram for Astaloy CrM (Fe-3%Cr-0.5%Mo) + 0.4% C.

Application of high temperature sintering in the production of PM steel parts, which usually means sintering at a temperature of 1200°C or above, gives a boost in mechanical performance compared to sintering at the conventional temperature 1120°C. The positive effect of high sintering temperature on the properties of Cr-Mo prealloyed PM steel has been demonstrated in several studies [22-24]. Typical improvements obtained for these materials when sintering at 1230-1250°C compared to 1120°C are 10-30% higher tensile strength, 20-30% higher fatigue strength, about 100% higher impact strength, and elongation to fracture values boosted from around 1% up to 2-4%. This is exemplified by the properties of Astaloy CrM obtained for two different sintering temperatures (1120/1250°C) shown in Figure 8. The results in Figure 8 also demonstrate the combined effect of warm compaction (to reach higher part density) and high temperature sintering on the mechanical performance of this PM steel.

The main reason for the positive effect of higher sintering temperature on the mechanical properties of PM steel is supposed to be that the pores become rounder and somewhat smaller. This can also be accomplished by using longer sintering time. Rounding of the pores means that they are less likely to act as crack initiators when the PM part is subjected to loading [25]. Furthermore, the pores can be considered as defects and decreased pore size is thus beneficial for the mechanical performance of PM steel. The pore size also decreases with increasing PM part density, which explains the correlation between density and mechanical properties shown in Figure 6. Another way to decrease the pore size is to use powder with smaller mean particle size. Hereby, large improvement in the fatigue strength of PM steel can be achieved [26].

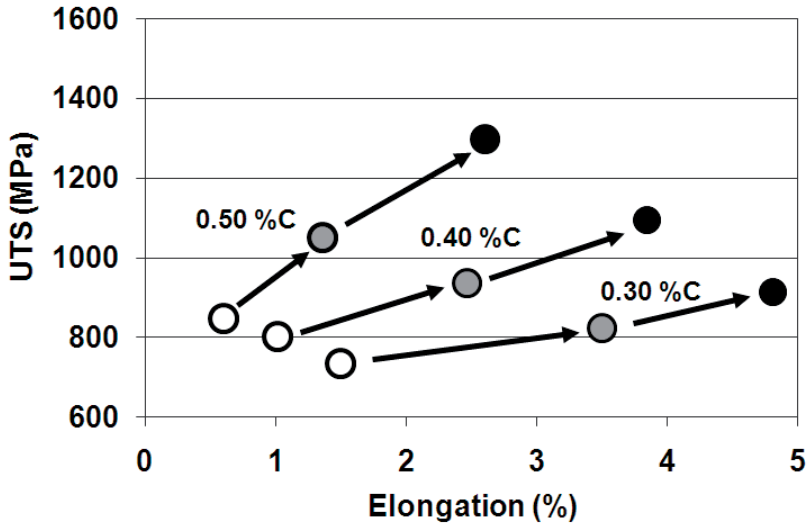

White circles: CC 600 MPa, T = 1120°C → density 6.9 g/cm^3
Grey circles: CC 600 MPa, T = 1250°C → density 7.0 g/cm^3
Black circles: WC 800 MPa, T = 1250°C → density 7.3 g/cm^3

Figure 8. Influence of sintering temperature (T) and part density on mechanical properties of the PM steel grade Astaloy CrM (with 0.3-0.5% C added). Sintering was done for 30 min at T and cooling rate after sintering was 1°C/s. Based on data from [22].

2.6 Applications for PM steel components

The global iron and steel powder production amounted to about 1.25 million metric tons in the year 2006 [27]. The produced powder volumes dropped significantly in Western Europe and North America during the financial crisis in 2008-2009, but recovery in these markets during 2010 and a continuous growth in Asia mean that yearly global volumes are similar or slightly higher today than in 2006.

Almost 80% of the produced iron and steel powder is converted into PM components, while the remaining share goes to, for instance, chemical and metallurgical applications, iron fortification of food and surface coatings. The PM steel components are used in many different applications such as power tools, white goods, lawn-mowers, air-conditioners, computers, locks and pumps. The automotive industry is the dominant user of PM steel parts with about 75% of the total tonnage, and most of these components are used in engine and transmission applications. In 2005, the typical US automobile contained over 20 kg of PM steel components, while a car fabricated in Europe or Japan contained about 40% of that amount in average [28]. Examples of components made from PM steel for different types of applications are displayed in Figure 9.

Spiral bevel gear for power tool.

Lawn mower part.

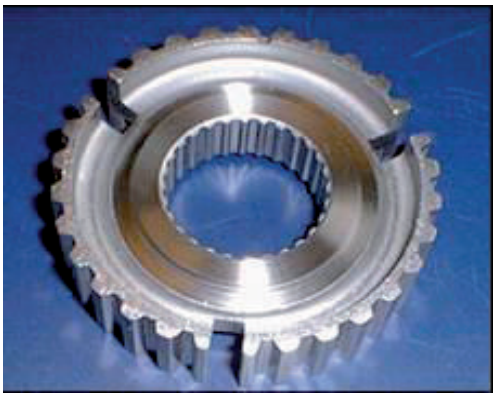

Synchronizing hub for automotive manual transmission.

Timing sprocket for automotive engine.

Figure 9. Examples of PM steel components for different applications.

3. Research Topic and Aim of the Work

Sintering is a crucial process step in the route for manufacturing of PM steel components. In the sintering process, bonding between adjacent powder particles in the compacted green body occurs through the formation of sinter necks, as illustrated schematically in Figure 10. The necking between the iron or steel particles starts during the heating stage when diffusion rates for the metal atoms become sufficiently high, which is at temperatures above around 800°C [29, 30]. Growth of the sinter necks then progresses during the isothermal hold time at the sintering temperature, which is usually in the range of 1120-1250°C, and mechanical strength is thereby provided to the PM component. Consequently, efficient sinter neck formation between the metal particles during sintering is essential for successful manufacturing of high-strength PM steel parts.

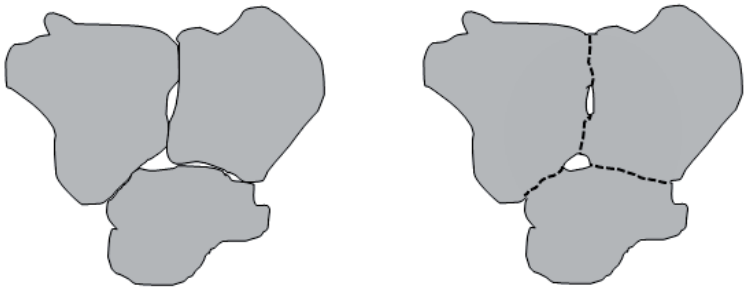

Before sintering *After sintering*

Figure 10. Schematic illustration of the formation of sinter necks (marked by dashed lines) between powder particles in a PM steel compact during sintering (author's illustration).

A prerequisite for efficient formation of sinter necks under the processing conditions applied in sintering of PM steel is that surface oxides on the powder particles are reduced to ensure metal-to-metal contact between the particles [11-13]. For pure Fe powder and steel powder grades that contain alloying elements with low oxidation sensitivity (e.g. Mo and Ni), the surface oxides are reduced at lower temperatures before the sinter neck formation starts. However, for powder grades prealloyed with oxidation sensitive elements such as Cr and Mn, there are thermodynamically stable oxides on the powder surfaces that require higher reduction temperatures. It is thus important to gain knowledge about the mechanisms for oxide reduction in these powder grades during sintering in order to clarify the role of surface oxides on the sinter neck formation in the material. Sintering atmosphere requirements regarding critical oxygen levels for reduction must also be established, since oxidation during sintering might obstruct the development of the sinter necks. Furthermore, understanding of how residual oxides after sintering affect mechanical properties of PM steel grades prealloyed with Cr and Mn is of importance for the applicability of these materials.

The aim of the performed research work has been to build a fundamental knowledge platform regarding sintering process requirements for successful manufacturing of PM steel components from powder grades prealloyed with Cr and Mn. The main focus has been to study the key aspects discussed above, namely:

- *Sintering atmosphere requirements regarding critical oxygen levels.*
- *Mechanisms for reduction of surface oxides on the powder particles during sintering.*
- *Effects of residual oxides after sintering on mechanical properties of the PM steel.*

The test materials used in the research studies have been two commercial powder grades prealloyed with 1.5-3% Cr and 0.2-0.5% Mo, a recently developed powder grade prealloyed with 1.8% Cr, and an experimental powder grade prealloyed with 0.8% Cr and 0.4% Mn. Test specimens of various sizes and with different densities were used in sintering experiments in order to investigate how transport processes inside the porous PM compacts affect the oxide reduction for these powder grades. The sintering temperature has been the process parameter of main interest in the studies of the oxide reduction mechanisms, since both reduction reactions and transport processes are greatly affected by the temperature. Moreover, sintering experiments in atmospheres with different oxygen partial pressures have been performed in order to study the atmosphere requirements for reduction. All sintering trails have been conducted in mixed N_2/H_2 atmosphere, as this is the prevailing industrial practise for oxidation sensitive PM grades. The experimental work is described in more detail in chapter 5, where also the applied analysis techniques are presented.

Thermodynamic calculations have been performed in order to gain information about the stability of oxides in the investigated material systems. This information has been a valuable tool in the interpretation of results from the experimental work, especially for identification of oxide phases and their reduction temperatures. The calculations have also been shown to be very useful for prediction of critical oxygen levels for reduction in the sintering atmosphere. A theoretical background for the thermodynamic calculations is presented in chapter 4 together with some calculation results on oxide stabilities. In the same chapter, descriptions are given of the reactions for oxide reduction during sintering as well as of the critical transport and diffusion mechanisms involved in the reduction process.

The results from the performed research studies are summarized in chapter 6. This summary is divided into three sections in accordance with the key aspects that have been investigated regarding sintering of PM steel prealloyed with Cr and Mn. Main conclusions from the research work is presented in chapter 7 and suggestions for future work in the field are given in chapter 8.

4. Theoretical Considerations on Oxide Reduction during Sintering

4.1 Surface oxides on powder

Water-atomized steel powder is covered by surface oxides due to reactions between metallic elements and water vapour or oxygen during the atomization process. The composition and structure of the surface oxides depend on the steel chemistry and the atomization process parameters. Steel alloys containing strong oxide forming elements are particularly sensitive for oxidation and higher demands are put on the atomization process for these alloys than for e.g. pure Fe. However, protective measures during atomization can only limit the oxidation to a certain degree and elements with high affinity for oxygen will inevitably form thermodynamically stable oxides on the powder surfaces. It has for example been demonstrated that water-atomized austenitic stainless steel powder is covered by surface oxide layers with thickness of around 10 nm that are rich in Si as well as Cr and Mn [31-33]. In fact, surface oxides with similar characteristics may appear also when gas-atomization is applied as production method; it has been shown that gas-atomized martensitic stainless steel powder is covered by a Cr and Mn rich oxide layer with an average thickness of about 7 nm [34].

Surface oxides on water-atomized and subsequently annealed low-alloy steel powder containing Cr and Mn have been characterized in several investigations. Studies of steel powder prealloyed with 1.5-3% Cr and 0.2-0.5% Mo show that there are oxide particulate features rich in both Cr and Mn evenly distributed on the surfaces and these features are surrounded by a continuous Fe oxide layer [35-38]. These powder grades also contain about 0.1% Mn, which explains the presence of Mn in the surface oxide features. The surface oxide characteristics are similar for steel powder prealloyed with 0.3-1.8% Mn and up to 0.3% Cr [29, 39]. However, the oxide particulate features are richer in Mn and contain less Cr on these powders than on the Cr-Mo prealloyed powders. The thickness of the continuous Fe oxide layer on the powder surfaces is typically around 6-7 nm while the Cr-Mn rich oxide particulates have a size of up to a few hundred nanometers, as demonstrated by the high-resolution SEM image in Figure 11. The oxide particulates cover a minor part of the powder surfaces. It has been estimated in a recent investigation that in average around 5-6% of the surface area of a powder particle is covered by these types of oxide particulates [29].

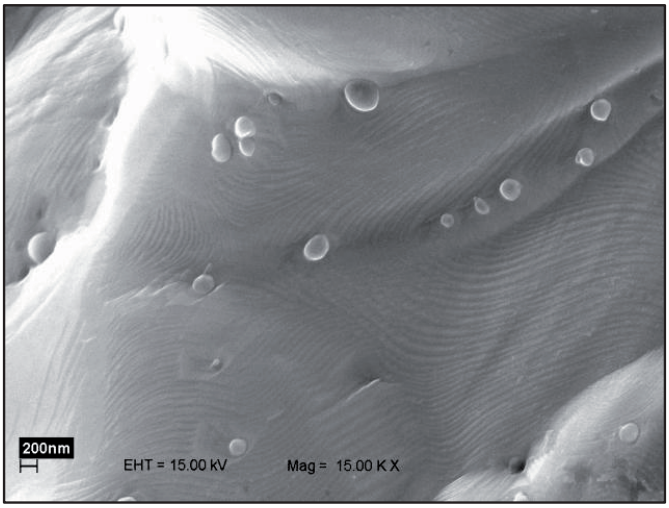

Figure 11. High-resolution SEM image of 3%Cr-0.5%Mo prealloyed steel powder particle showing the presence of small (sub-micrometre size) surface oxide particulate features (from the work by Chasoglou et al. [37]).

4.2 Thermodynamic stability of oxides

Thermodynamic calculations can be applied to determine the relative stability of metal oxides. The reaction between a metal *M* and oxygen for the formation of an oxide proceeds according to the following reaction:

$$xM(s) + yO_2(g) \rightarrow M_xO_{2y}(s) \tag{5}$$

The standard Gibbs free energy change for this reaction is defined as:

$$\Delta G^0 = \Delta H^0 - T \cdot \Delta S^0 = -R \cdot T \cdot \ln(K) \tag{6}$$

where ΔH^0 is the standard enthalpy change, ΔS^0 is the standard entropy change, R is the molar gas constant and T is the absolute temperature. The equilibrium constant, K, is the ratio of the activities of the reaction products to the reactants:

$$K = \frac{a_{M_xO_{2y}}^{1/y}}{a_M^{x/y} \cdot a_{O_2}} \tag{7}$$

The activities of the solid phases may be assumed to be equal to unity and the activity level of oxygen can be replaced by the oxygen partial pressure (p_{O2}). Hence, the standard Gibbs free energy change for the formation of an oxide according to reaction (5) is then given by expression (8) below.

$$\Delta G^0 = \Delta H^0 - T \cdot \Delta S^0 = R \cdot T \cdot \ln\left(p_{O_2}\right) \qquad (8)$$

This equation can be used together with tabulated values for ΔH^0 and ΔS^0 to plot ΔG^0 versus temperature for metal-oxide systems in a so called Ellingham diagram [40], whereby an overview is obtained of the thermodynamic stability of different oxide phases. Richardson and Jeffes [41] introduced a p_{O2} scale in the Ellingham diagram which provides the possibility to estimate the critical oxygen partial pressure for reduction of a specific oxide at a given temperature, as demonstrated in Figure 12. This is done by drawing a straight line from point "O" in the upper left corner of the diagram to the ΔG^0 line of the metal-oxide system in question at a point corresponding to the given temperature. Point "O" corresponds to $\Delta G^0(T = 0\text{K}) = 0$ and the slope of the line is given by $R \cdot \ln(p_{O2})$ in accordance with equation (8). The intersection between the extension of this line and the p_{O2} scale on the right-hand side of the diagram gives the critical pressure for reduction, which in the case of the Cr-Cr_2O_3 system is $p_{O2} \sim 10^{-15}$ atm at temperature 1200°C.

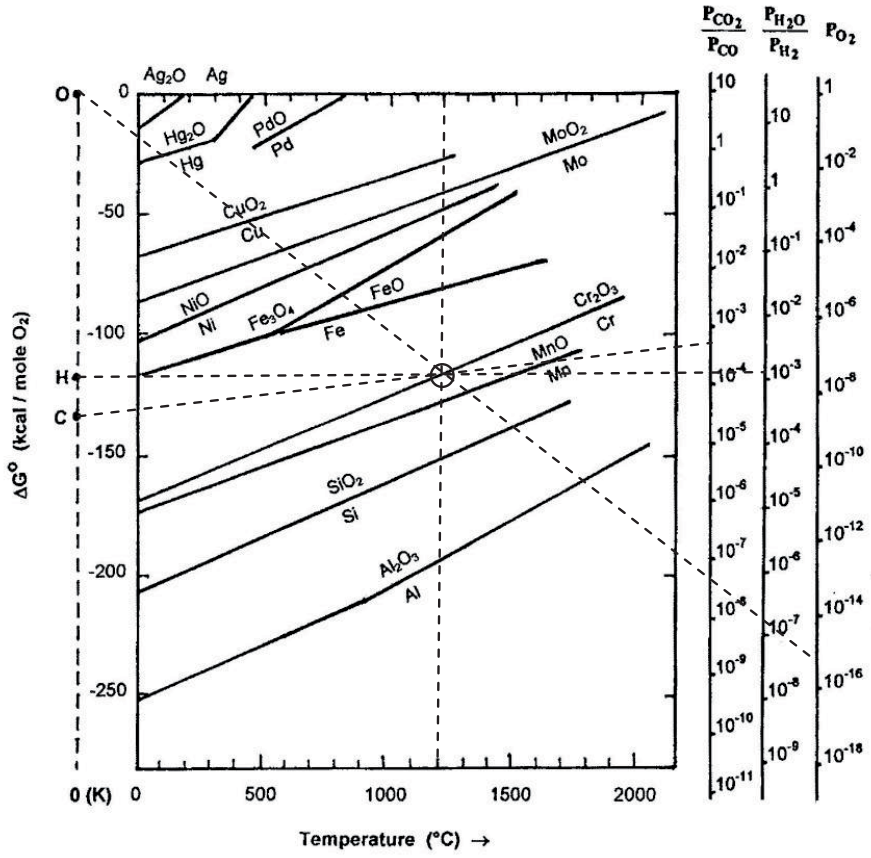

Figure 12. Ellingham-Richardson diagram with ΔG^0 lines for different metal-oxide systems. The dashed lines show critical values of p_{O2}, p_{CO2}/p_{CO} and p_{H2O}/p_{H2} for reduction in the system Cr-Cr_2O_3 at the temperature 1200°C. The diagram is redrawn from [42].

There are also scales for p_{CO2}/p_{CO} and p_{H2O}/p_{H2} on the right-hand side of the Ellingham-Richardson diagram in Figure 12. The ratios between the partial pressures of CO_2-CO and H_2O-H_2 represent the equilibrium constants for oxidation of a metal by CO_2 and H_2O, respectively. These oxidation reactions are given by the reversed reactions (9) and (11) in the next sub-chapter, and the equilibrium constants for the reactions are thus the activity or pressure ratios for the involved gas species. Estimations of critical p_{CO2}/p_{CO} and p_{H2O}/p_{H2} ratios for reduction of a specific oxide can be extracted from the diagram in similar way as for critical p_{O2} values. Lines are in this case extended from point "C" to the p_{CO2}/p_{CO} scale and from point "H" to the p_{H2O}/p_{H2} scale, through the ΔG^0 line of the metal-oxide system in question at a point corresponding to a given temperature. For the Cr-Cr_2O_3 system at 1200°C, it can be estimated that the critical ratios for reduction are $p_{CO2}/p_{CO} \sim 10^{-3}$ and $p_{H2O}/p_{H2} \sim 10^{-3}$ as demonstrated in Figure 12.

The method described above is useful for the prediction of oxide stabilities in relation to pure metals. However, the situation is more complex when Fe-based alloys are considered, since the alloying elements are in solid solution in the Fe matrix which lowers the activity of the elements. For accurate predictions of oxide stabilities in multi-component material systems more advanced thermodynamic calculations are needed. The computer software Thermo-Calc [43] is a very helpful tool for such calculations, which has been utilized in the performed research work to consider the stability of oxide phases in the investigated alloy systems. The accuracy of phase stability calculations with Thermo-Calc depends on the applied thermodynamic database. Calculations of oxide stabilities in the Fe-Cr-O-(C) system have been performed with the database CCTOX, which was developed within the Swedish research programme Centre for Computational Thermodynamics. The commercial thermodynamic steel database TCFE6.2 has been applied for stability calculations of oxide phases in the system Fe-Cr-Mn-O. This database contains new and improved data for mixed Fe-Cr-Mn oxides. The improved data originate from a recently developed thermodynamic description of the Fe-C-Cr-Mn-Ni-O system [44].

Thermo-Calc calculations show that two different oxides are thermodynamically stable in steel alloyed with 3% Cr at 1120°C and 1250°C for oxygen partial pressures below 10^{-13} atm, as illustrated by Figure 13. The Cr_2O_3 oxide is stable at the lowest oxygen partial pressures, while the spinel oxide $FeCr_2O_4$ is stable at somewhat higher oxygen pressures. Furthermore, the stability of the oxides is shifted to higher oxygen pressures when the temperature increases. The results in Figure 13 also provide critical oxygen partial pressures for oxide reduction during sintering of PM steels pre-alloyed with 3% Cr. The critical pressures are $p_{O2} = 4 \cdot 10^{-18}$ atm at 1120°C and $p_{O2} = 1 \cdot 10^{-15}$ atm at 1250°C. The former value is well in accordance with the recommendation based on experimental results of a maximum p_{O2} of $5 \cdot 10^{-18}$ atm when sintering such steels at 1120°C [45]. For a steel alloy with lower Cr content (1.5%) the critical oxygen partial pressures for oxide reduction during sintering are slightly higher ($p_{O2} = 1 \cdot 10^{-17}$ atm at 1120°C and $p_{O2} = 3 \cdot 10^{-15}$ atm at 1250°C), as demonstrated from Thermo-Calc results in Paper II. Hence, PM steel pre-alloyed with 1.5% Cr is somewhat less sensitive for oxidation during sintering than PM steel pre-alloyed with 3% Cr, which is due to lower Cr activity in the former material.

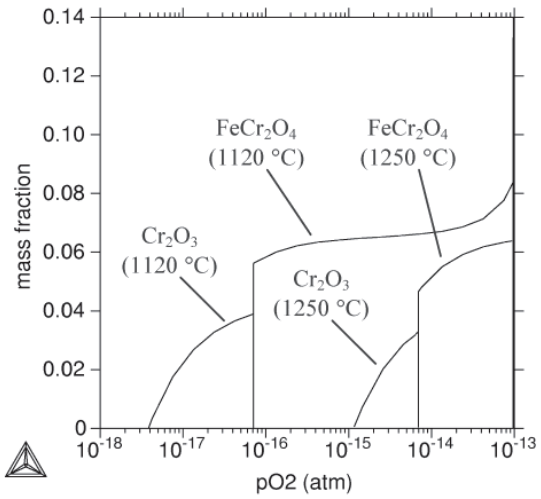

Figure 13. Mass fraction of stable oxide phases versus oxygen partial pressure at 1120/1250°C for a steel alloy with composition Fe-3%Cr-0.35%C (from Paper I).

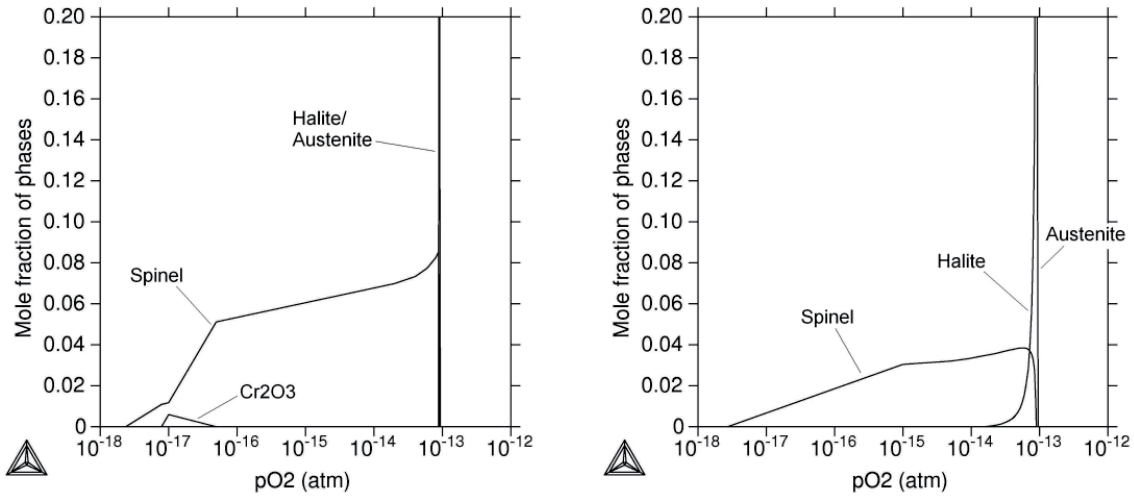

Fe-1.8%Cr-0.1%Mn Fe-0.8%Cr-0.4%Mn

Figure 14. Mole fraction of stable phases versus oxygen partial pressure at 1120°C for two different steel alloy compositions (from Paper IV).

The presence of small amounts of Mn in low-alloy steel containing Cr leads to stabilization of the spinel oxide phase. This is demonstrated by the Thermo-Calc results from Paper IV that are displayed in Figure 14. For both the alloy compositions Fe-1.8%Cr-0.1%Mn and Fe-0.8%Cr-0.4%Mn, the $MnCr_2O_4$ spinel is the most stable oxide phase and an oxygen pressure below $p_{O2} = 3 \cdot 10^{-18}$ atm is required for reduction of this oxide at 1120°C. Consequently, the critical oxygen partial pressure for oxide reduction during sintering is basically the same for pre-alloyed PM steel with these chemical compositions as for PM steel pre-alloyed with 3% Cr (see Figure 13).

The equilibrium composition of the spinel phase in the steel alloys in Figure 14 varies with p_{O2} and goes from being Cr-Fe rich at high oxygen pressures to being stoichiometric $MnCr_2O_3$ at the lowest critical p_{O2} value, as shown in Paper IV. The strong stability of this spinel oxide is in line with results from surface analysis of powder where Cr-Mn rich oxide features have been shown to exist on the surfaces of different powder alloys containing Cr and Mn, as discussed in the previous sub-chapter. Experimental results from various oxidation trials have also demonstrated that oxide scales formed on Fe-Cr-Mn steel alloys tend to contain $MnCr_2O_3$ or $(Cr,Mn,Fe)_3O_4$ spinel, often together with the chromium oxide Cr_2O_3 [46-49].

Calculations with Thermo-Calc can also provide valuable information about temperature stability ranges for different oxide phases in a steel at fixed oxygen partial pressure. This is exemplified by the graphs in Figure 15 where the amount of stable phases is given as function of temperature at constant p_{O2} for two different alloy compositions. The graphs show that the temperature should be above ~1050°C in order to have reducing conditions for the alloy Fe-3%Cr at $p_{O2} = 10^{-19}$ atm, while a temperature above ~1100°C is required for having reducing conditions for the alloy Fe-1.8%Cr-0.1%Mn at $p_{O2} = 10^{-18}$ atm.

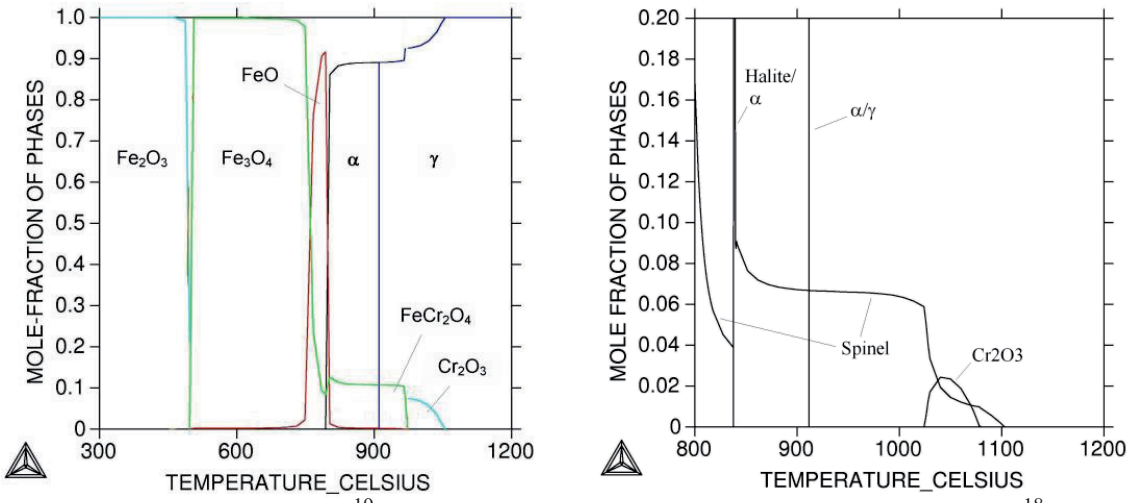

Fe-3%Cr, $p_{O2} = 10^{-19}$ atm Fe-1.8%Cr-0.1%Mn, $p_{O2} = 10^{-18}$ atm

Figure 15. Mole fraction of stable phases versus temperature at fixed oxygen partial pressure for two different steel alloy compositions (from Paper III and Paper V, respectively).

From thermodynamic calculations it is thus possible to obtain the demands put on the sintering process, in terms of combination of temperature and oxygen partial pressure, for having reducing conditions in the processing of oxidation sensitive PM alloys. However, for understanding of how oxides on the powder surfaces are reduced during sintering it is necessary to also consider reduction reactions and transport processes inside the PM parts. These subjects are treated in the next two sub-chapters.

4.3 Reduction reactions

Reduction of metal oxide (M_xO_y) on the powder surfaces in the sintering process can occur through interaction with H_2 in the sintering atmosphere according to reaction (9) below. Alternatively, carbothermal reduction occurs through interaction between the oxide and carbon according to reaction (10). Carbon is added to the metal powder in the form of graphite before compaction. The CO gas generated in reaction (10) can also interact with the oxide to cause in-direct carbothermal reduction according to reaction (11).

$$M_xO_y(s) + yH_2(g) \rightarrow xM(s) + yH_2O(g) \quad (9)$$

$$M_xO_y(s) + yC(s) \rightarrow xM(s) + yCO(g) \quad (10)$$

$$M_xO_y(s) + yCO(g) \rightarrow xM(s) + yCO_2(g) \quad (11)$$

The carbothermal reduction starts in accordance with reaction (10) when the temperature is high enough to activate the graphite in the powder compact. However, as soon as CO becomes available reaction (11) will be the main reduction mechanism, and regeneration of CO is ensured at high temperatures by the Boudouard reaction [50-52]:

$$C(s) + CO_2(g) \rightarrow 2CO(g) \quad (12)$$

Combination of the hydrogen reduction reaction (9) and the in-direct carbothermal reduction reaction (11) yields the water-gas shift reaction, which is catalyzed by many metals and oxides [53]:

$$CO(g) + H_2O(g) \leftrightarrow CO_2(g) + H_2(g) \quad (13)$$

No kinetic model for description of reaction rates in the reduction of oxides on surfaces of Cr-Mn-alloyed steel has been found in the literature. However, a kinetic model for oxidation/reduction of iron in CO_2-CO and H_2O-H_2 mixtures has been presented by Grabke [54]. According to this model, the following rate equation applies for the removal of adsorbed oxygen atoms in the case of carbothermal reduction through reaction (11):

$$v_1 = k_1 \cdot a_0^{-m} \cdot p_{CO2} \left[\frac{a_0}{p_{CO2}/p_{CO}} - 1\right] \quad (14)$$

where k_1 is a rate coefficient, a_0 is the oxygen activity at the surface of the oxide, and m is a reaction exponential (m = 0.66 for wustite). Equation (14) describes reduction if the activity $a_0 > p_{CO2}/p_{CO}$ and otherwise oxidation. The hydrogen-assisted oxide reduction in accordance with reaction (9) is described by two rate equations, since the removal of adsorbed oxygen atoms through interaction with H_2 consists of three sub-reactions whereof the two first might be rate determining; see reaction sequence (15).

$$O(ad) + H_2(g) \overset{k_2'}{\rightarrow} OH(ad) + H(ad) \overset{k_2''}{\rightarrow} H_2O(ad) \rightarrow H_2O(g) \qquad (15)$$

The two rate equations are as follows:

$$v_2' = k_2' \cdot a_0^{-n'} \cdot p_{H2O}/p_{H2}^{1/2} \left[\frac{a_0}{p_{H2O}/p_{H2}} - 1\right] \qquad (16)$$

$$v_2'' = k_2'' \cdot a_0^{-n''} \cdot p_{H2O} \left[\frac{a_0}{p_{H2O}/p_{H2}} - 1\right] \qquad (17)$$

where k_2' and k_2'' are rate coefficients whereas n' and n'' are reaction exponentials. These equations describe reduction if the oxygen activity at the oxide surface $a_0 > p_{H2O}/p_{H2}$ and otherwise oxidation. The values of the rate coefficients in equations (14), (16) and (17) vary with type of oxide, temperature, and the pressure ratios p_{CO2}/p_{CO} and p_{H2O}/p_{H2}, respectively. For example, the value of k_1 is in the order of 10^{-8}-10^{-9} mol·cm^{-2}·s^{-1}·atm^{-1} during oxide formation of wustite on Fe at 800-900°C and $p_{CO2}/p_{CO} \sim 1$ atm [54]. It is unclear whether the rate coefficients are in the same order of range during reduction of oxides on the surfaces of Cr-Mn-alloyed steel powder in the sintering process.

Oxide reduction mechanisms during sintering of PM compacts based on powder prealloyed with 3% Cr and 0.5% Mo have been studied in several investigations [55-57]. These studies show that H_2 reduction of iron oxides on the powder surfaces occurs in the temperature range of 300-600°C during heating in N_2/H_2 atmosphere. Carbothermal reduction is initiated at around 700°C, which is attributed to further iron surface oxide reduction. More intense carbothermal reduction takes place above ~900°C when thermodynamically stable Cr-rich oxides on the powder surfaces are reduced. Reduction maxima for these oxides are obtained at temperature ranges of 1000-1050°C and 1200-1250°C. Similar oxide reduction sequence has been reported from sintering trials with PM compacts based on powder prealloyed with 0.3-1.2% Cr and 0.8-1.2% Mn [58]. In this case, large carbothermal reduction peaks with maxima at 1200-1250°C are obtained due to removal of stable Cr-Mn oxides.

The fact that effective carbothermal reduction of Cr-rich oxide on powder surfaces can be achieved at a temperature of 1200°C is supported by results from a study on sintering of pressed specimens based on stainless steel powder (Fe-19%Cr-11%Ni) mixed with graphite [59]. Here, sintering at 1200°C for 30 minutes in vacuum resulted in complete reduction of such surface oxides. The results agree fairly well with findings from investigations of the carbothermal reduction process for Cr_2O_3 [60, 61]. During heating of mixtures of Cr_2O_3 powder and graphite in streaming helium, the reduction starts at a temperature of about 1000°C, maximum reduction rate is reached at around 1150°C, and the reduction is completed just above 1200°C.

All of the mentioned studies of oxide reduction during sintering were performed on test specimens with density around 7.0 g/cm^3, which means that there is open and interconnected porosity in the PM compacts that allows transport of the gas species that take part in the reduction reactions (9)-(11). In another investigation, oxide reduction during sintering of high density (7.5-7.6 g/cm^3) PM compacts based on powder prealloyed with 1.5% Cr and 0.2% Mo was studied [62]. The oxide reduction in these specimens is virtually stopped at temperatures above 1150°C due to closing of the pore channels, and thereby stable Cr-Mn-rich oxides remain in the material even after heating to 1300°C. Consequently, successful reduction of the surface oxides during sintering requires that gas species involved in the reduction process can be efficiently transported through the pore system of the PM compact. The role of gas diffusion through the pores on the oxide reduction process is treated further in the next sub-chapter.

4.4 Transport and diffusion processes

Consider a compacted PM specimen based on water-atomized steel powder prealloyed with Cr and Mn. Continuous layers of easily reduced Fe oxides on the powder surfaces are removed during heating early in the sintering process, as described in the previous sub-chapter, ensuring metal-to-metal contact between powder particles. Bonding between powder particles starts to occur at a temperature of around 800°C. Discrete thermodynamically stable Cr-Mn oxide particulate features still remain on the powder surfaces at this temperature, which means that some of these oxides will be entrapped inside sinter necks while the rest of the oxides will be situated on the surfaces of the pore walls. The pores are either open and interconnected with the surrounding sintering atmosphere or closed and isolated from any gas exchange with the sintering atmosphere. An illustration of how the stable oxide features can be distributed inside a PM compact is presented in the schematic picture in Figure 16.

Reduction of the Cr-Mn oxides will progress through carbothermal reduction in accordance with the described reduction process in the previous sub-chapter. The final reduction product is CO gas, which the results from performed reduction trials have demonstrated [55-58], and this CO has to be transported out of the PM compact by gas diffusion through the open pore system. Furthermore, reduction of entrapped oxides or oxides in closed pores requires that diffusion of atomic oxygen occurs through the steel matrix to open pores, where the oxygen can react and form CO gas. These diffusion processes are illustrated in Figure 16.

The critical transport processes involved in the reduction of the Cr-Mn oxide particulate features inside a PM specimen during sintering are thus the oxygen diffusion through the steel matrix to open pores and the CO gas diffusion through the pore system of the specimen. Descriptions of these processes including equations for estimation of diffusion rates are presented in the proceeding pages.

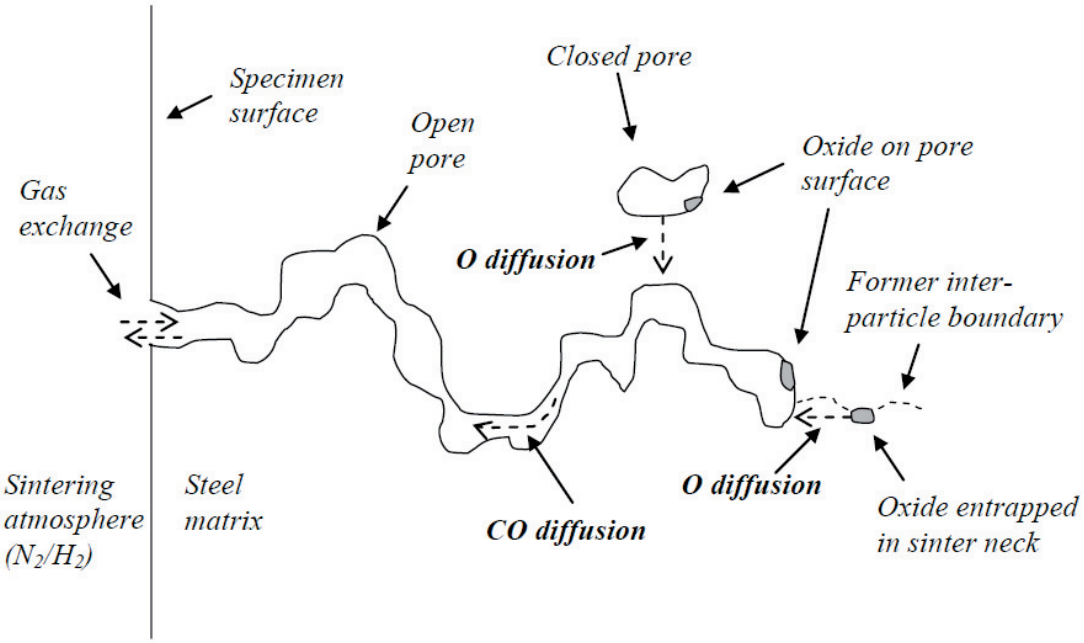

Figure 16. Schematic picture illustrating transport processes involved in the reduction of stable Cr-Mn oxides in a PM compact during the sintering process (from Paper V).

A general equation for description of the diffusion of atoms (or molecules) along a direction x is Fick´s first law:

$$J = -D \cdot \frac{\delta c}{\delta x} \tag{18}$$

where J is the flux of atoms (per unit area and unit time), D is the diffusion coefficient, and c is the concentration of atoms. The diffusion coefficient is a measure of the diffusion rate and $\delta c/\delta x$ expresses the concentration gradient along the x direction. This concentration gradient is the driving force for the diffusion. For diffusion in solids, the following expression shows how the diffusion coefficient is dependent on the absolute temperature T, the molar gas constant R, and the activation energy Q (D_0 is a frequency factor):

$$D = D_0 \cdot e^{-\frac{Q}{RT}} \tag{19}$$

Derivation of equations (18) yields Fick´s second law, which predicts how diffusion causes the concentration to vary with time t (for a closed system where no atoms are added or lost):

$$\frac{\delta c}{\delta t} = D \cdot \frac{\delta^2 c}{\delta x^2} \tag{20}$$

Oxygen diffusion through the steel matrix

In the course of a carbothermal reduction process inside a PM specimen, it can be assumed that a microclimate is formed around entrapped oxide particles as CO and CO_2 are formed through reactions (10) and (11). Production of CO and CO_2 also occurs inside closed pores when oxides on the pore walls are reduced. The adsorption of oxygen atoms on the metal surface may proceed through the dissociation of CO_2, which is an important mechanism for transfer of oxygen from CO_2-CO mixtures to the metal surface during oxidation of iron [54]:

$$CO_2(g) \rightarrow CO(g) + O(ad) \tag{21}$$

There should now be a driving force for diffusion of the adsorbed oxygen atoms to nearby pore surfaces in the open porosity, provided that these pore surfaces are oxygen-free and in contact with a reducing atmosphere. Oxygen diffuses interstitially through the metal lattice and the atoms are therefore capable of moving fast at high temperatures [63]. The diffusion coefficient D_{ox} for oxygen in γ-iron has been determined by Takada et al. [64] and it may be expressed as in equation (22), which is a re-written form of equation (19) with given values of the frequency factor and the activation energy.

$$D_{ox} = 1.30 \cdot 10^{-4} \cdot \exp\left[-\frac{166(kJ \cdot mol^{-1})}{R \cdot T}\right] m^2 \cdot s^{-1} \tag{22}$$

$$L = 2 \cdot \sqrt{D_{ox} \cdot t} \tag{23}$$

From expression (22) and equation (23) for calculation of diffusion length L, it is possible to estimate the diffusion time t for transport of oxygen atoms through the metal during sintering. The value of the diffusion coefficient is D_{ox} = $8 \cdot 10^{-7}$-$3 \cdot 10^{-6}$ cm^2/s for typical sintering temperatures in the range of 1120-1250°C. The time for diffusion is then only 0.1-0.3 s for a diffusion length of 10 μm and 2-8 s for a diffusion length of 50 μm, where the longest diffusion time is for the lower temperature in the respective case. These diffusion lengths represent estimations of typical distances from entrapped oxides in sinter necks and oxides on surfaces of closed pores, respectively, to surfaces of open pores (see Figure 16). Hence, the oxygen diffusion through the steel matrix should proceed quickly during sintering, provided that there is a driving force for the diffusion and that there are enough diffusion paths for diffusion of the atoms.

CO diffusion in the pore system

The following equation is commonly used for calculation of the effective diffusion coefficient (D_{eff}) for gas diffusion in a porous medium [65]:

$$D_{eff} = \frac{\varepsilon}{\tau} \cdot D_{gas} \tag{24}$$

where ε is the open porosity of the medium, τ is the tortuosity of the pore system, and D_{gas} is the diffusion coefficient for the gas.

The value of D_{gas} in equation (24) depends on whether collisions between the gas molecules and the pore walls have significant influence on the diffusion process, in which case Knudsen diffusion dominates, or if only collisions between gas molecules themselves have to be accounted for as in the case of molecular (or Fickian) gas diffusion. The dominant type of diffusion can be determined from the Knudsen number (Kn), which is given by the ratio of the mean free path (λ) of the gas molecules to the mean pore radius (r_m):

$$Kn = \frac{\lambda}{r_m} \tag{25}$$

Knudsen diffusion dominates if Kn is much larger than 1 whereas the diffusion is mainly Fickian if Kn is much smaller than 1. If Kn is near or equal to 1 there is transition-mode diffusion with properties of both Knudsen and Fickian diffusion. The mean free path of a gas molecule can be calculated from:

$$\lambda = \frac{k_B \cdot T}{\sqrt{2} \cdot \pi \cdot d^2 \cdot p} \tag{26}$$

where k_B is the Boltzmann constant, T is the absolute temperature, d is the diameter of the gas molecule, and p is the pressure. With the values $k_B = 1.38 \cdot 10^{-23}$ J/K, $d_{CO} = 3.76 \cdot 10^{-10}$ m and p = 1 atm = $1.01 \cdot 10^5$ Pa, equation (26) shows that the mean free path for CO gas molecules is λ_{CO} = 0.30-0.33 μm in the temperature range 1120-1250°C. It has been estimated from microstructures of PM specimens with densities of 7.0-7.3 g/cm^3 (see Paper V) that r_m for open pores is somewhere between 5 μm and 10 μm. Using these values in equation (25), the Knudsen number is in the range Kn = 0.03-0.07 and thereby it should be reasonable to only consider the Fickian diffusion of CO in the pore system of PM steel specimens with densities up to 7.3 g/cm^3 when sintering at temperatures between 1120-1250°C.

Binary diffusion coefficients D_{AB} for a gas pair A-B are applicable in the Fickian diffusion regime. A widely used equation for the prediction of such coefficients is that of Fuller-Schettler-Giddings [66]:

$$D_{AB} = \frac{1.00 \cdot 10^{-3} \cdot T^{1.75} \cdot \sqrt{\frac{1}{M_A} + \frac{1}{M_B}}}{p \cdot \left[(\Sigma v)_A^{1/3} + (\Sigma v)_B^{1/3} \right]^2} \tag{27}$$

where T is the absolute temperature, M_A and M_B are the molecular weights of the gas molecules (in g/mol), p is the pressure (in atm), and $(\Sigma v)_A$ and $(\Sigma v)_B$ are so called diffusion volumes for the two gas molecules that have dimensions of atomic volumes. The atmosphere in the pores of a PM specimen should be equal to the sintering atmosphere, which is usually N_2-based in the processing of Cr-Mn-alloyed steel grades. Hence, the most appropriate gas pair should be CO-N_2 in this context. The diffusion volumes for these gas species are $(\Sigma v)_{CO}$ = 16.80 and $(\Sigma v)_{N2}$ = 17.92 [66].

The tortuosity τ of the pore system is a factor which characterizes the convoluted nature of the porous pathways followed by the diffusing species. According to the random-pore model developed for predicting diffusion rates through catalyst pellets, the tortuosity may be expressed as the inverse of the open porosity [67]:

$$\tau = \frac{1}{\varepsilon} \tag{28}$$

This expression has in a later study [68] shown relatively good agreement with experimental results for highly sintered pellets with low porosity (<10%), although the calculated tortuosity values are slightly underestimated. By combining equations (24) and (28) the expression for calculation of the effective diffusion coefficient for CO in the pore system of a PM specimen is as follows, where $D_{CO\text{-}N2}$ is given by equation (27):

$$D_{eff} = \varepsilon^2 \cdot D_{CO-N2} \tag{29}$$

The open porosity ε of PM compacts can be estimated from their total porosity if no measured values are available. According to information given by Thümmler and Oberacker [69], about half the porosity is open at 10-11% total porosity while only about one quarter of the porosity is open at around 8% total porosity. Below around 7% total porosity, which corresponds to a density of 7.35 g/cm^3 for a PM steel compact with full theoretical density 7.9 g/cm^3, there is virtually no open porosity. A somewhat higher compact density (7.45-7.5 g/cm^3) for the transition between semi-open and completely closed porosity has been reported from a study of Cr-Mo prealloyed PM steel [70].

In Paper V, equation (29) was applied for calculations of the effective diffusion coefficient for CO transport during sintering in the pore system of PM specimens with two different densities (7.0/7.3 g/cm^3). These calculations show that the sintering temperature in the range of 1120-1250°C has relatively small influence on the diffusion rate of CO. However, the effective diffusion coefficient values are one order of magnitude smaller at the specimen density 7.3 g/cm^3 (D_{eff} = 1·10^{-3} cm^2/s) compared to the density 7.0 g/cm^3 (D_{eff} = 1·10^{-2} cm^2/s), which demonstrate that the CO gas transport in the pore system should have significantly higher limiting effect on the oxide reduction process during sintering at the higher specimen density level than at the lower.

5. Experimental Work

5.1 Investigated materials

Four different water-atomized steel powder grades have been investigated in the performed research work. Two of the powder grades are prealloyed with Cr and Mo, one is prealloyed with Cr only, and one is prealloyed with Cr and Mn. The first three are commercial powder grades (Astaloy materials) while the fourth material is an experimental powder grade (termed AD4). All the grades have standard <250 μm particle size distribution. The chemical compositions of the powder grades are given in Table 2.

Table 2. Nominal chemical compositions (in wt%) of investigated powder grades.

Powder Grade	Fe	Cr	Mo	Mn	O	C
Astaloy CrM	Base	3.0	0.5	0.1	<0.2	<0.01
Astaloy CrL	Base	1.5	0.2	0.1	<0.2	<0.01
Astaloy CrA	Base	1.8	-	0.1	<0.2	<0.01
AD4	Base	0.8	-	0.4	<0.2	<0.01

The powder grade Astaloy CrM was used as test material in the research studies presented in Paper I, Paper II and Paper III. The research work presented in Paper II also included Astaloy CrL as test material. Both Astaloy CrA and the experimental grade AD4 were investigated in the research study presented in Paper IV, while only Astaloy CrA was used as test material in the research work presented in Paper V. In one of the research studies (Paper IV), the commercial water-atomized steel powder grade Astaloy Mo, which is prealloyed with 1.5 wt% Mo, was included in the investigation as reference material. The powder mixes produced in the experimental studies have been based on the investigated steel powder grades and they have also contained additions of graphite and lubricant. The natural graphite grade Kropfmühl UF4 was used and the graphite content in the test mixes was up to 0.85 wt%. The amount of lubricant in the mixes was in the range of 0.5-0.8 wt% and the lubricant type was either amide wax, Kenolube or Lube E.

Manufacturing of test specimens from the powder mixes has been done by conventional uniaxial compaction. Cold compaction with compaction pressures between 600 and 700 MPa was applied to produce specimens with green density of 6.9-7.1 g/cm^3. Warm die compaction with a pressure of 800 MPa was used to produce specimens with green density of 7.2-7.3 g/cm^3, and double pressing with the compaction pressures 700/900 MPa was applied to produce specimens with green density of 7.5 g/cm^3. Pre-sintering was done at 750°C for 30 minutes in $75H_2/25N_2$ between the two compaction steps in the double pressing operation. The specimen types used in the investigations have been standard tensile test specimens (ISO 2740-1986) and un-notched impact tests specimens (ISO 5754), as well as cylindrical specimens with diameter 25 mm and height 20 mm.

5.2 Performed sintering trials

An overview of the process parameters used in the performed sintering trials is presented in Table 3. The trials are described briefly below for each of the conducted studies.

Table 3. Process parameters applied in performed sintering trials.

Paper No	HR (°C/s)	T (°C)	t (min)	CR (°C/s)	Purity of N_2/H_2 atmosphere*
I	30	1120/1250	30	0.3/2.0	$p_{O2}=10^{-16}$-10^{-18} atm
II	30	1120/1200/1250	30	0.5/2.5	DP < -40°C
III	30	1120/1250	30	-**	DP ~ -60°C
	5	1300	10		
IV	30	1120/1200/1250	30	0.5-1.0	DP < -40°C
V	30	1120/1200/1250	30	-**	DP ~ -60°C
	5	1300	10		

HR = heating rate, T = sintering temperature, t = time at T, CR = cooling rate
**) Normally $90N_2/10H_2$, **) Cooling rate was not analysed*

The sintering trials for the research study described in Paper I were performed in a laboratory tube furnace. This equipment consists of a Kanthal APM tube (inner diameter 200 mm) and a programmable furnace that controls the temperature cycle in the heating zone. In these experiments, test specimens were placed on a vessel attached to a rod by which the vessel could be pushed to transport the specimens through the furnace tube. De-waxing of the test specimens was done in the heating zone of the tube furnace at 600-700°C for 30 minutes, where after the specimens were heated to the sintering temperature with a rate of around 30°C/minute. Hold time at sintering temperature (1120-1250°C) was 30 minutes in all experiments. Different cooling rates after sintering were achieved by pushing the vessel holding the test specimens, out of the heating zone and through a second heating zone set at 600°C, at a speed corresponding to the desired cooling rate. The gas flow through the furnace tube was 4-5 litres per minute in all sintering trials. Small additions of synthetic air were made to a high purity N_2/H_2 (90/10) mixture to obtain sintering atmospheres with different oxygen partial pressures; c.f. Table 3. An oxygen probe and a dew point analyser were used to monitor the process atmosphere purity in the heating zone.

Two different laboratory sintering furnaces were applied for the sintering trials that are reported on in Paper II and Paper IV; a batch furnace and a mesh belt furnace. The batch furnace can be used for sintering experiments at high temperatures (up to at least 1300°C), while trials in the mesh belt furnace are restricted to a maximum temperature of about 1150°C. In the batch furnace, vessels containing the test specimens are loaded on a carousel set-up that is elevated into the heating zone (size 500x500x700 mm) and cooling after sintering is achieved by lowering the set-up carrying the specimens out of the heating zone into a cooling chamber. The gas flow through the furnace is set to 100 litres per minute during sintering trials. The heating rate to sintering temperature is about 5°C/min in

this furnace. In the continuous belt furnace (see Figure 17), vessels carrying the test specimens are transported on a mesh belt inside the furnace muffle (internal cross section size 200x100 mm) through the heating zone and onwards through a cooling zone, which is equipped with convective cooling capacity for sinter-hardening of the specimens. The protective atmosphere flows at a rate of about 100 litres per minute continuously through the muffle in the opposite direction to the movement of the mesh belt during sintering trials. The heating rate for the specimens in this furnace is about 30°C/min. In both furnaces, an oxygen probe or a dew point analyser continuously measures the oxygen level/dew point of the protective atmosphere in the heating zone during the sintering cycle.

Figure 17. Laboratory mesh belt furnace used for sintering trials in the research studies described in Paper II and Paper IV.

For the investigation presented in Paper II, sintering of the test bars was performed in the laboratory batch furnace for 30 minutes at different temperatures (1120-1250°C) in a N_2/H_2 (90/10) atmosphere with dew point below -40°C. Cooling rate after sintering was 0.5°C/s in the interval 700-300°C. All test specimens of Astaloy CrM were re-sintered in the laboratory belt furnace (1120°C, 30 min, $90N_2/10H_2$), where sinter-hardening was performed with a cooling rate of 2.5°C/s in the interval 650-250°C. The sinter-hardened samples were tempered at 200°C for 60 minutes in air.

Also for the research study presented in Paper IV, sintering trials were performed both in the mesh belt furnace (1120°C for 30 min) and in the batch furnace (1200/1250°C for 30 min). All specimens from the sintering trials in the batch furnace were re-sintered in the mesh belt furnace (1120°C for 30 min) in order to ensure that the same cooling rate after sintering was applied for all materials. This cooling rate was between 0.5°C/s and 1°C/s in the temperature range 300-800°C. High purity $90N_2/10H_2$ gas mixture (dew point < -40°C) was used as protective atmosphere in all sintering trials.

The sintering trials for the investigations presented in Paper III and Paper V were conducted in a laboratory quartz tube furnace with an inner tube diameter of 35 mm. The test specimens were heat treated for lubricant removal, either at 700°C for 30 minutes in $75H_2/25N_2$ or at 600°C for 30 minutes in pure N_2, before the sintering trials. In these trials, a single specimen was placed on a vessel inside the heating zone of the furnace and the temperature cycle was controlled by the programmable furnace. A continuous gas flow (5 liters per minute) of mixed N_2/H_2 (90/10) or H_2 was used as furnace atmosphere in the experiments. The gas was supplied from cylinders containing high purity instrumental gas (dew point ~ -60°C). Outgoing gas from the furnace tube was analyzed by a photoacoustic spectroscopy (PAS) instrument for concentrations down to around 1 ppm of the gas species H_2O, CO, CO_2 and CH_4 (information about the PAS technique is given in the next sub-chapter). Trials with slow heating (5°C/min) to 1300°C followed by 10 minute isotherm were done in both investigations as well as simulated sintering trials with 30 minute isotherm at 1120/1200/1250°C (the isotherm at 1200°C was only tested in the second investigation). The heating rate in the simulated sintering trials was 30°C/min up to a temperature of 800-1000°C (depending on the isotherm temperature), after which the heating rate was lower (5-10°C/min) in order to avoid over-temperature at the isotherm. Cooling of the sample after sintering was done in an un-heated part of the furnace tube with the same process gas flowing. The cooling rate was not controlled in these trials.

5.3 Applied analysis techniques

Chemical analysis

Chemical analysis of bulk contents of oxygen and carbon in sintered materials was carried out in instruments equipped with infrared detector in all investigations. For the determination of O content, a sample of approximately 1 g is placed in a graphite crucible and melted in an induction furnace under a flow of helium gas. The oxygen released by the sample reacts with carbon from the crucible to form CO and CO_2. These gas species are registered by the IR detector, which gives the O content of the sample. For determination of C content, a sample of approximately 1 g is combusted in an induction furnace in a flow of oxygen gas, whereupon the carbon in the sample is transformed into CO and CO_2. In this case, registration of the CO and CO_2 gas species by an IR detector gives the C content of the sample.

Density measurements

Density measurements on test samples were performed with the aid of Archimedes' principle in accordance with the standard ISO 2738:2000. By measuring the weight of a test sample in air and in water, the density of the sample can be determined from this principle. Sintered samples were impregnated before the weight measurements in order to prevent water from entering the pores.

Gas analysis

Photoacoustic spectroscopy (PAS) was applied in the investigations presented in Paper III and Paper V for analysis of the composition of the outgoing gas from the furnace tube in the sintering trials. The PAS instrument used for the gas analysis is calibrated for measurements of very low concentration levels of the gas species CO (0.2-2000 ppm), CO_2 (1.5-2000 ppm), CH_4 (0.4-2000 ppm), and H_2O (0.1-1000 ppm) [71]. In the PAS unit, a gas sample is exposed to infrared (IR) light whereupon the gas absorbs certain wavelengths corresponding to the resonant vibration frequency of the different gas molecules. Optical filters are used to expose the sample to the IR wavelengths necessary for excitation of the specific gas molecules. Pressure waves are generated when relaxation of the gas molecules occurs and these waves are detected as acoustic signals by microphones inside the measurement chamber. The acoustic signals are directly proportional to the concentrations of the analyzed gas species. The PAS instrument does not analyze the gas continuously, since a closed measurement chamber is required to register the pressure variations. The time between gas sample collections in the sintering trials was about 60 seconds.

Metallography

Microstructures of the sintered test specimens were studied by light optical microscopy (LOM) in all investigations. Cross sections of the specimens were examined in as-polished state as well as after etching. The etchant used was 100 ml ethyl alcohol (95%) with addition of either 1 ml concentrated HNO_3 or 2 g picric acid and 1 ml concentrated HCl.

Fractography

In the research study presented in Paper IV, high-resolution scanning electron microscopy (HR-SEM) was applied in a LEO Gemini 1550 instrument for examination of fracture surfaces of tensile test specimens. Particulate features in the fracture surfaces were analyzed by energy dispersive X-ray spectroscopy (EDX) through an INCA system in combination with the SEM instrument. The principle of the SEM technique is that an electron beam emitted from an electron gun is scanned over the sample inside a vacuum chamber. The energy exchange between the electron beam and the sample results in the reflection of electrons by elastic scattering (back-scattered electrons), the emission of secondary electrons by inelastic scattering, and the emission of characteristic X-rays. The X-rays are emitted when electrons from an outer higher-energy electron shell of an atom, which has been excited by the incident electron beam, fill the holes in an inner electron shell. Specialized detectors are used to register the different types of emissions from the sample. By secondary electron imaging the SEM instrument can produce high-resolution images of the sample surface, revealing details of only a few nm in size. Back-scattered electron imaging can be used to provide information about the distribution of different elements in the sample. An EDX analysis of the X-rays emitted from the sample gives information about the chemical composition at the analysis point of the sample. The information depth of this analysis is usually in the μm range and is determined by the size of the teardrop-shaped interaction volume from the incident electron beam.

Mechanical testing

Evaluation of mechanical properties of sintered specimens was done in accordance with ISO standard methods in the research studies presented in Paper I, Paper II and Paper IV. The Vickers method was applied to determine the hardness of the materials. The hardness measurements were done either on polished cross sections of test specimens or on specimen surfaces. Tensile tests were performed on 7-10 tensile test specimens from each test series to evaluate ultimate tensile strength (UTS), yield strength (YS) and elongation to fracture (A). A Charpy impact tester was used to determine the impact strength, given by the impact energy (IE) absorbed during fracture. The impact tests were performed on 5-10 un-notched specimens for each material series.

6. Summary of Results

6.1 Sintering atmosphere requirements

The influence of oxygen partial pressure in the protective atmosphere during sintering on the properties of Cr-Mo prealloyed PM steel was studied in the investigation presented in Paper I. The aim of the study was to establish critical oxygen levels in the protective atmosphere for successful sintering of the steel powder grade Astaloy CrM. Tensile test specimens with green density 7.0 g/cm^3 were used for the sintering trials.

The results from this investigation demonstrate that conditions are reducing for an oxygen pressure of $p_{O2} = 10^{-18}$ atm in the atmosphere when sintering Astaloy CrM specimens (without graphite) at 1120°C, as illustrated by the graph in Figure 18. However, conditions are not reducing in atmospheres with $p_{O2} = 10^{-16}$-10^{-17} atm at the same sintering temperature. This is in agreement with thermodynamic equilibrium calculations which show that reducing conditions prevail for $p_{O2} < 4 \cdot 10^{-18}$ atm at 1120°C for a steel alloyed with 3% Cr (see Figure 13). The prediction from equilibrium calculations of a higher critical oxygen level ($p_{O2} < 10^{-15}$ atm) during sintering at 1250°C is also supported by the results from the performed study. Hence, sintering atmosphere requirements regarding critical oxygen partial pressures for oxide reduction can be well-predicted by thermodynamic calculations in accordance with what was outlined in sub-chapter 4.2.

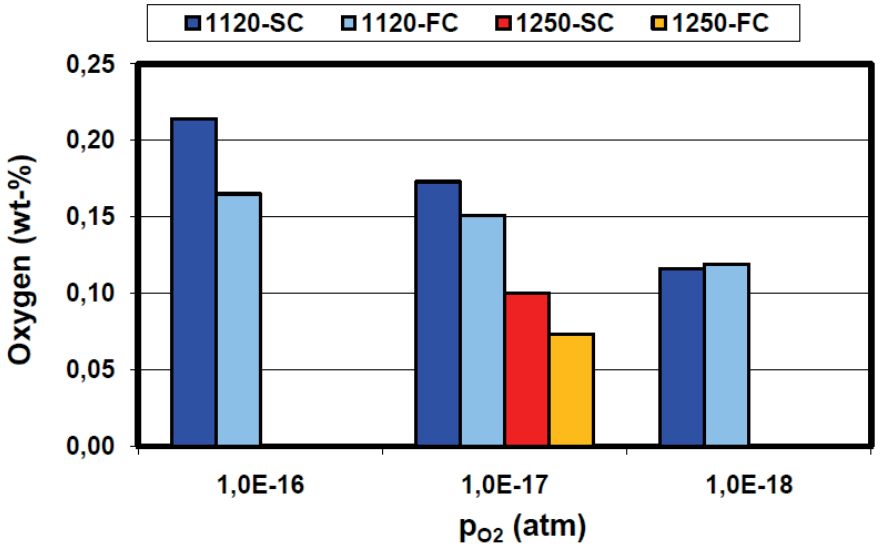

Figure 18. Oxygen contents in test bars (density 7.0-7.1 g/cm^3) based on Astaloy CrM (without graphite) after sintering at 1120/1250°C for 30 min in N_2/H_2 (90/10) with different p_{O2}. Cooling rates were 0.3°C/s (SC) and 2.0°C/s (FC). Oxygen content of the powder was 0.16 wt% before sintering. Graph is taken from Paper I.

The results from the study described in Paper I also show that oxides are reduced in Astaloy CrM specimens containing 0.35% C during sintering at 1120°C although p_{O2} in the protective atmosphere is above the critical thermodynamic equilibrium pressure. This effect is attributed to favourable CO/CO_2 ratios locally in the specimens that drive the carbothermal oxide reduction in accordance with reaction (11) in sub-chapter 4.3. However, the specimens sintered in atmospheres with oxygen levels above the critical value for reduction are subjected to surface decarburization due to reaction between oxygen in the atmosphere and carbon in the specimen. Such decarburization might de detrimental for the mechanical performance of the PM steel and should be avoided. The decarburizing effect of high oxygen levels in the sintering atmosphere could possibly be counteracted by using small additions of CH_4 or CO as described in sub-chapter 2.4. Still, sintering atmosphere requirements should be based on the critical oxygen partial pressures predicted by thermodynamic calculations in order to avoid the risk of oxidation as well as surface decarburization of the PM steel compacts. As the calculation results presented in sub-chapter 4.2 show, the critical oxygen pressure is in the range of $p_{O2} = 10^{-17}$-10^{-18} atm when sintering at 1120°C for all four PM steel alloys that were investigated in the performed research studies.

6.2 Oxide reduction mechanisms

Oxide reduction during sintering of the Cr and Mn containing prealloyed PM steel grades has been investigated in all of the performed research studies. In the studies presented in Paper I and Paper II, information about the reduction process has been gained by analysing bulk oxygen contents in sintered specimens and examining residual oxides in the specimen microstructures. This was also done in the study presented in Paper IV, where additional information was retrieved by EDX analysis of oxide features in fracture surfaces of sintered specimens. The oxide reduction mechanisms were more thoroughly investigated in the studies presented in Paper III and Paper V, where PAS analysis of the atmosphere composition during sintering has been utilized to study the reduction reactions.

The PAS analysis results in Paper III from sintering trials with cylindrical test specimens (GD = 6.9 g/cm^3) of Astaloy CrM + 0.5% C provide information about how the oxide reduction proceeds (see Figure 19). These results show, with knowledge about the characteristics of surface oxides on the investigated powder grade, that the continuous Fe oxide layer on the powder surfaces is reduced by H_2 from the sintering atmosphere in accordance with reaction (9) early in the heating stage of the process. Moreover, thermodynamically stable oxide particulate features on the powder surfaces are reduced by interaction with C in the material through the carbothermal reactions (10) and (11). This carbothermal reduction process starts at a temperature of around 900°C and a reduction maximum is reached just above 1200°C, as shown by the slow heating trial results. The results in Paper III further demonstrates that the reduction of the stable oxide particulate features is incomplete after sintering at 1120°C for 30 minutes, while practically complete reduction of these oxides is achieved after sintering at 1250°C for 30 minutes.

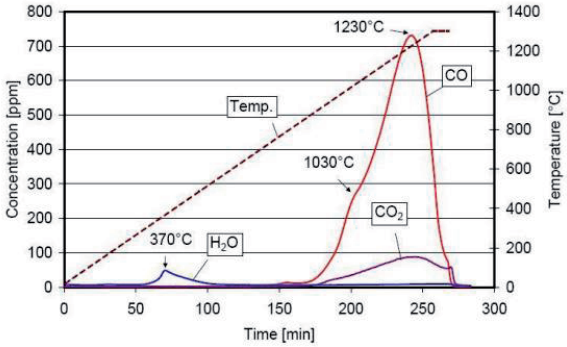

Trial 1: Slow heating to 1300°C.

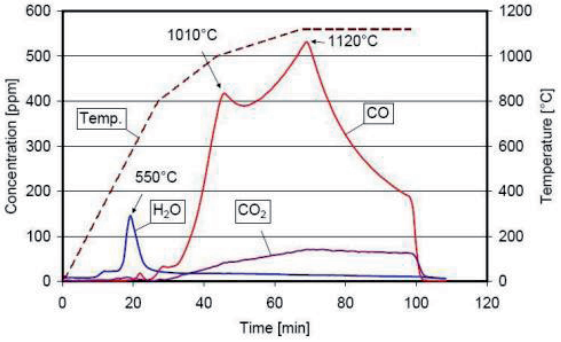

Trial 2: Sintering at 1120°C for 30 min.

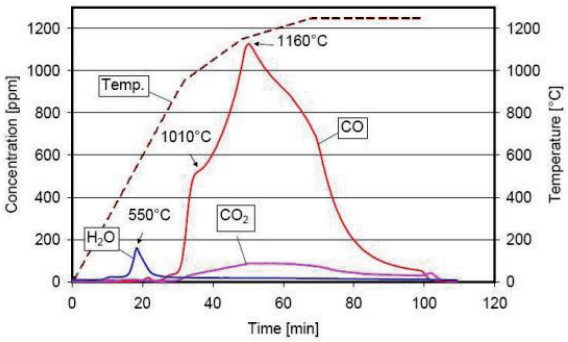

Trial 3: Sintering at 1250°C for 30 min.

Figure 19. Results from gas analysis by PAS in oxide reduction trials on test specimens (GD = 6.9 g/cm^3) of Astaloy CrM + 0.5% C in 90N_2/10H_2 atmosphere (from Paper III).

The results from the PAS measurements presented in Paper V from sintering trials with cylindrical test specimens (GD = 7.0 g/cm^3) of Astaloy CrA + 0.5% C are very similar to the results from Paper III shown in Figure 19. Consequently, the oxide reduction process during sintering is comparable for the two powder grades, which is logical since the materials should have basically the same surface oxide characteristics (see sub-chapter 4.1). The particulate features on the powder surfaces of these types of prealloyed powder are Cr-Mn rich oxides. Such oxide features are also found encapsulated inside sinter necks of Astaloy CrA + 0.5% C specimens after sintering at 1120°C as demonstrated in Paper IV (see Figure 20). The EDX analysis results indicate that these are Cr-Mn spinel oxides, which is in agreement with the oxide stability calculations presented in Figure 14. Results from the studies presented in Paper IV and Paper V show that sintering at 1120°C for 30 minutes leads to reduction of the stable Cr-Mn oxides on pore surfaces in a specimen with mainly open porosity, while stable oxide particulates that are encapsulated inside sinter necks or closed pores of the specimen largely remain after sintering. Furthermore, sintering at 1200/1250°C for 30 minutes enables reduction of the encapsulated oxides, provided that there is open and interconnected porosity available for transportation of the reduction product (CO gas) out of the specimen. The reduction of encapsulated oxides is more efficient at 1250°C than at 1200°C.

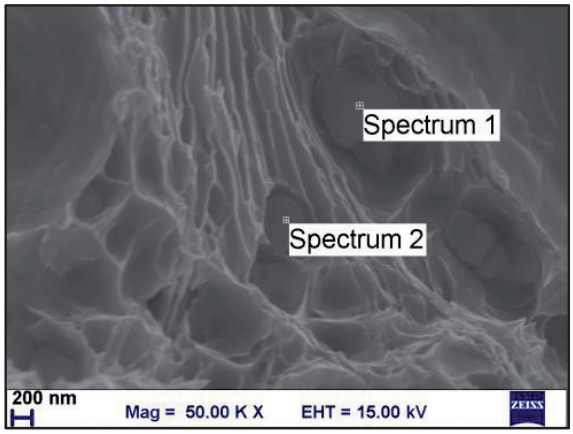

EDX analysis results in atomic % (Normalized)

	O	Si	Cr	Mn	Fe
Spectrum 1	43.8	1.0	19.8	10.5	24.8
Spectrum 2	42.9	2.3	11.3	5.3	38.2

Figure 20. SEM image of the fracture surface of TS specimen (Astaloy CrA + 0.8%C) sintered at 1120°C for 30 minutes in $90N_2/10H_2$. EDX analysis results are shown for oxide particulate features found inside sinter neck. From Paper IV.

The effect of specimen density on the oxide reduction process is demonstrated by the research results presented in Paper IV and PaperV. These results show that the reduction process is greatly affected by the specimen density between 7.0 g/cm^3 (mainly open porosity) and 7.5 g/cm^3 (completely closed porosity), which is illustrated by the PAS analysis results obtained from sintering trials at the isothermal temperature 1250°C with cylindrical specimens (ϕ = 25 mm, h = 20 mm) of Astaloy CrA + 0.5% C (see Figure 21). This is a consequence of the impact of the amount of open porosity on the effective CO diffusion rate in the pore system of the PM specimen, as described in sub-chapter 4.4. The effective CO diffusion rate is relatively high in a specimen with density 7.0 g/cm^3, which means that basically all oxides are reduced at distances of up to at least 10 mm from the specimen surfaces when sintering at 1250°C for 30 minutes. In the same sintering process the reduction depth decreases to about 5 mm for a specimen with density 7.3 g/cm^3, due to less effective CO diffusion in the specimen pore system. Very little reduction of the stable Cr-Mn oxides occurs in a specimen with density 7.5 g/cm^3 during sintering at 1250°C, since complete pore closure stops the CO diffusion in the specimen pore system.

Bulk oxygen contents in impact test specimens with quadratic cross sections (10×10 mm) from the sintering trials presented in Paper IV further illustrates the results described above (see Figure 22). In this case, there are no significant differences in the amount of oxides reduced during sintering between specimens with density 7.0 g/cm^3 and those with density 7.3 g/cm^3. The maximum reduction depth in these specimens is 5 mm and thereby the difference in effective CO diffusion rate between the two porosity levels does not affect the overall reduction process. However, very limited oxide reduction is achieved at all sintering temperatures also for these specimens at density 7.5 g/cm^3 due to complete closure of the pore system.

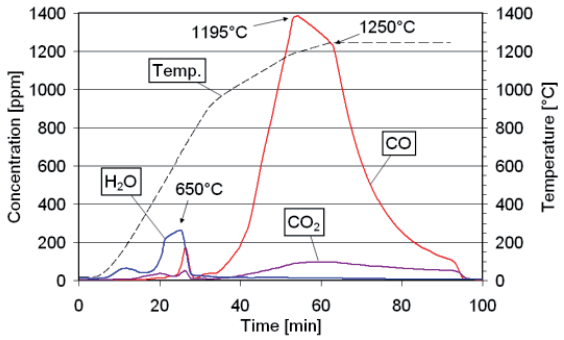

Specimen green density: 7.0 g/cm^3

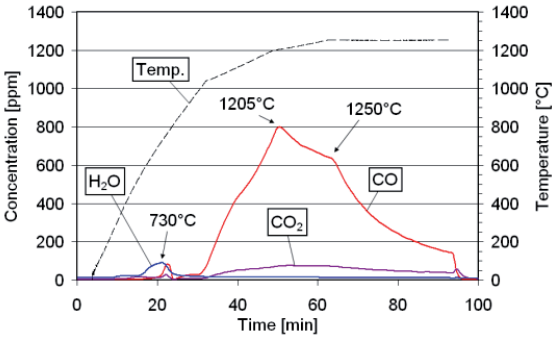

Specimen green density: 7.3 g/cm^3

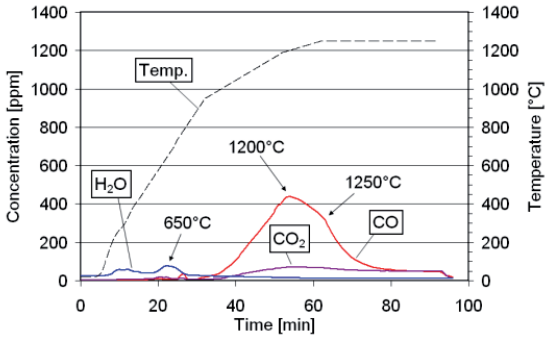

Specimen green density: 7.5 g/cm^3

Figure 21. Results from gas analysis by PAS in sintering trials (1250°C, 30 min, $90N_2/10H_2$) on cylindrical test specimens of Astaloy CrA + 0.5% C (from Paper V).

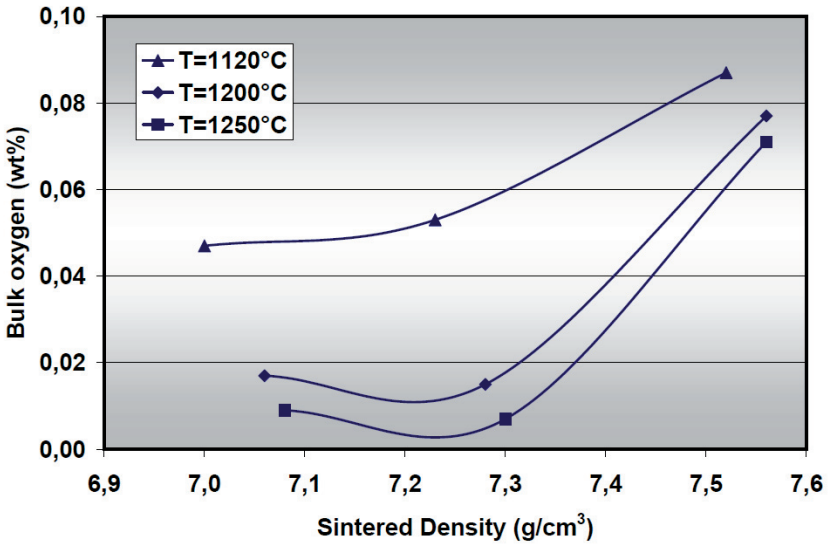

Figure 22. Bulk oxygen content in impact test specimens of Astaloy CrA + 0.8% C after sintering for 30 minutes at T in $90N_2/10H_2$ atmosphere (from Paper IV).

The data presented in Figure 22 represent fairly well the bulk oxygen contents obtained in sintered specimens in all the conducted research studies, although somewhat higher oxygen contents (0.07-0.10%) are typically obtained in specimens with mainly open porosity after sintering at 1120°C.

6.3 Effects of residual oxides on mechanical properties

Mechanical properties of test bars from performed sintering trials have been evaluated in the research studies described in Paper I, Paper II and Paper IV.

The results presented in Paper I show that Astaloy CrM specimens (density ~7.0 g/cm^3) sintered in oxidizing atmospheres have less good mechanical performance than corresponding specimens sintered in reducing atmospheres. Specimens with very low carbon content (<0.1% C) and mainly ferritic microstructures show large variation in tensile strength (205-318 MPa) and particularly in elongation to fracture (2-12%) after sintering at 1120°C in atmospheres with different oxygen partial pressures. This variation can be attributed to the detrimental effect of large amounts of oxides along prior particle boundaries in specimens that were oxidized during sintering. As for the specimens containing 0.2-0.3% C with mainly bainitic microstructures, there are only small differences in mechanical performance (UTS, YS and elongation to fracture) between specimens sintered in different atmospheres. These specimens have considerable differences in surface hardness values. This is a consequence of the fact that specimens sintered in oxidizing atmospheres have been subjected to surface decarburization. Some improvement in tensile strength and elongation to fracture was achieved for specimens sintered at 1250°C compared to those sintered at 1120°C. This improvement should mainly be an effect of rounder pores and slightly higher density for the specimens sintered at the higher temperature. The fact that the specimens contain considerably more oxygen after sintering at 1120°C (0.08% O) than after sintering at 1250°C (0.01% O), due to less effective reduction of entrapped oxide particulate features, should not have any significant effect on the evaluated mechanical properties.

The positive effect of higher sintering temperature on the mechanical performance of PM steel based on Cr-Mo prealloyed powder is also demonstrated by the results presented in Paper II. Sinter-hardened specimens (density ~7.1 g/cm^3) of Astaloy CrM + 0.5% C with fully martensitic microstructures show some enhancement in tensile and yield strength as well as elongation to fracture with increasing sintering temperature from 1150 up to 1250°C. Also specimens (density 7.0-7.1 g/cm^3) of Astaloy CrL + 0.8% C with mixed pearlitic/bainitic microstructures display some enhancement in tensile and yield strength with increasing sintering temperature in the range from 1120°C to 1200°C. However, the strength values for these specimens were lower after sintering at 1240°C compared to after sintering at 1200°C, which is explained by changed microstructure due to lower carbon content in the material that was sintered at the highest temperature.

The impact strength increases continuously with the sintering temperature over the whole tested temperature range for both the Astaloy CrM specimens and the Astaloy CrL specimens, as shown by the data from Paper II presented in Figure 23. These results coincide with more effective oxide reduction in the specimens as the sintering temperature increases. After sintering at 1120-1160°C, the specimens contain 0.04-0.08% O and residual oxides are visible in the microstructures. The oxide content in the specimens is reduced to 0.01-0.02% after sintering at 1200-1250°C and only traces of residual oxides remain in the microstructures. However, the fact that the improvement in impact strength with increasing sintering temperature continuous above 1200°C although most oxides are already reduced at this temperature, indicates that the residual oxides have small influence on this material property. The pore rounding effect of using higher sintering temperature should be the main mechanism for the improvement in impact strength.

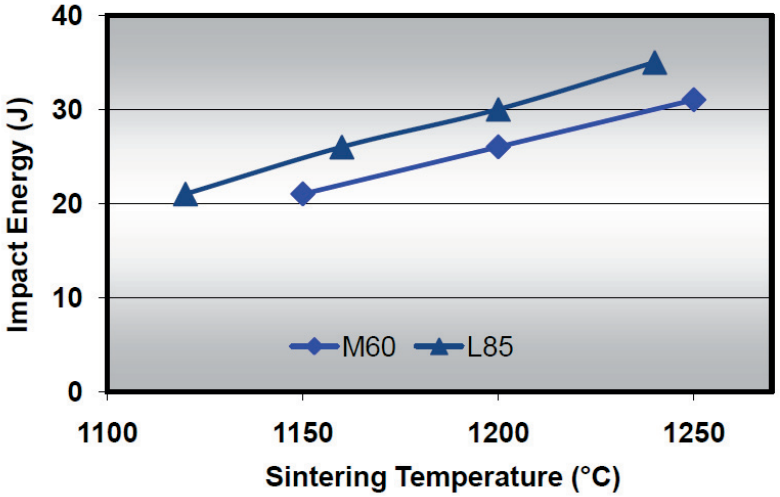

Figure 23. Impact strength obtained after sintering at different temperatures for 30 min in $90N_2/10H_2$ followed by rapid cooling (2.5°C/s) for M60 (Astaloy CrM + 0.6% C) and normal cooling (0.5°C/s) for L85 (Astaloy CrL + 0.85% C). From Paper II.

In Paper IV, mechanical properties are presented for test specimens with different densities (7.0-7.6 g/cm^3) of the grades Astaloy CrA and AD4 (both containing around 0.7% C after sintering). These specimens were sintered for 30 minutes at 1120-1250°C in $90N_2/10H_2$ atmosphere followed by normal cooling (0.5-1°C/s) resulting in fine pearlitic microstructures for both materials. All specimens sintered at 1120°C contain small residual oxide particles encapsulated inside the sinter necks, as demonstrated in Figure 20 in the previous sub-chapter. The high density (7.5-7.6 g/cm^3) specimens contain more such oxides than the specimens with lower densities, in line with the differences in specimen oxygen content (see Figure 22). After sintering at 1200-1250°C, the high density specimens still have residual oxides particles inside the sinter necks while the specimens with densities of 7.0-7.3 g/cm^3 have clean and basically oxide free sinter necks. There were no significant differences in oxygen content or amount of residual oxides between the two materials.

The results from the mechanical evaluation show that both materials gain considerably in mechanical performance with higher sintering temperature. Mechanical properties of the materials are also significantly improved with increasing specimen density throughout the density range 7.0-7.6 g/cm^3. This is exemplified by the elongation and impact strength values shown in Figure 24. There are no indications from these results that the residual oxides have any detrimental effect on the evaluated mechanical properties, which is supported by the similar trend in mechanical performance obtained for the oxide-free reference material. The positive effect of higher sintering temperature on the properties of the investigated materials is essentially due to pore rounding effects, increased sinter neck contact area, and slightly increased sintered densities. Furthermore, the improvement in mechanical performance with higher specimen density is in line with what can be expected from the effects of decreased overall porosity and smaller pore size.

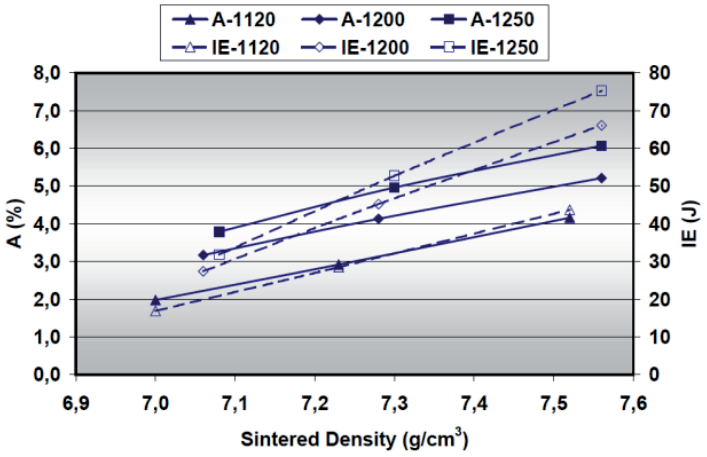

Astaloy CrA + 0.7% C

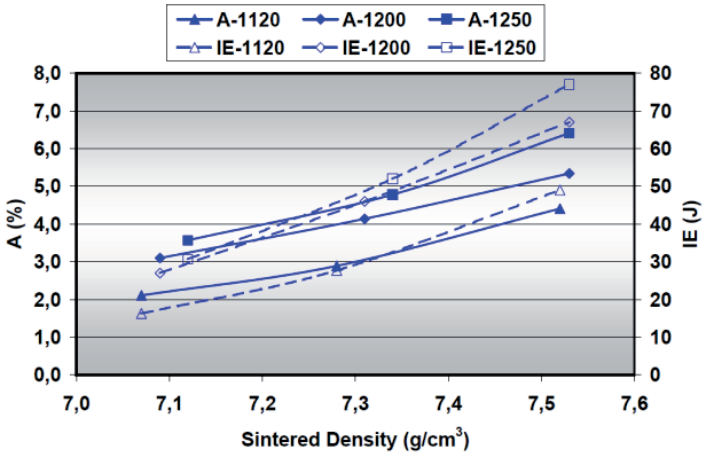

AD4 + 0.7% C

Figure 24. Mechanical properties obtained after sintering for 30 min at 1120/1200/1250°C in $90N_2/10H_2$ atmosphere (A = elongation to fracture, IE = impact energy). From Paper IV.

7. Main Conclusions

Main conclusions from the performed research work regarding key aspects of sintering PM steel prealloyed with Cr and Mn are summarized below. The investigated key aspects are sintering atmosphere requirements, oxide reduction mechanisms during sintering, and effects of residual oxides on mechanical properties of the sintered material. The conclusions are based on the results obtained from sintering trials with test specimens produced from water-atomized steel powder grades prealloyed with 3%Cr-0.5%Mo, 1.5%Cr-0.2%Mo, 1.8%Cr and 0.8%Cr-0.4%Mn.

Sintering atmosphere requirements

Sintering atmosphere requirements regarding critical oxygen partial pressures for oxide reduction can be well-predicted by thermodynamic calculations of oxide stabilities in the steel. The most stable oxide phases in the investigated alloys are Cr_2O_3 and the spinel oxide $MnCr_2O_4$. The critical oxygen partial pressure for reduction of these oxide phases when sintering at the temperature 1120°C is in the range of $p_{O2} = 10^{-17}$-10^{-18} atm for all four studied PM steel alloys.

Oxide reduction mechanisms

The reduction process in a PM compact proceeds as follows during sintering in reducing N_2/H_2 (90/10) atmospheres:

- The continuous iron oxide layer on the powder surfaces is reduced through reactions with H_2 from the atmosphere early in the heating stage of the process, which gives the prerequisites for an efficient sinter neck formation in the compact.
- Reduction of thermodynamically stable Cr-Mn rich oxides, which are in the form of micrometer size particulate features on the powder surfaces, occurs through carbothermal reactions at temperatures above around 1000°C.
- Sintering at 1120°C for 30 minutes leads to reduction of the stable Cr-Mn oxides on pore surfaces in a specimen with open porosity, while stable oxides that are encapsulated inside sinter necks or closed pores of the compact largely remain after sintering. Typical oxygen content in the material after sintering is 0.05-0.10%.
- Sintering at 1200/1250°C for 30 minutes enables reduction of the encapsulated oxide particles provided that the compact porosity is mainly open. The reduction of these oxides is more efficient at 1250°C than at 1200°C. Typical oxygen content in the material after sintering at these temperatures is 0.01-0.02%.
- The reduction of the Cr-Mn oxide particles is greatly affected by the compact density between 7.0 g/cm^3 (mainly open porosity) and 7.5 g/cm^3 (completely closed porosity), due to the impact of the amount of open porosity on the effective CO gas diffusion rate in the pore system. As a consequence, the reduction depth from the compact surfaces decreases from above 10 mm at density 7.0 g/cm^3 to about 5 mm at density 7.3 g/cm^3 when sintering at 1250°C for 30 minutes. The reduction of Cr-Mn oxides in a compact with density 7.5 g/cm^3 is very limited even during sintering at 1250°C, since complete pore closure stops the CO diffusion in the pore system.

Effects of residual oxides on mechanical properties

There are no indications from the performed studies that residual oxides, in the form of micrometer size particulate features inside sinter necks of sintered material, have any detrimental effect on the mechanical properties of the investigated PM steel grades. The materials gain considerably in mechanical performance with increased sintering temperature in the range between 1120°C and 1250°C in a process with 30 minutes hold time at temperature. The positive effect of higher sintering temperature is essentially due to pore rounding effects, increased sinter neck contact area, and slightly increased sintered density. Mechanical properties of the investigated materials are also significantly improved with increasing PM specimen density throughout the density range 7.0-7.6 g/cm^3. This improvement is in line with what can be expected from the effects of decreased overall porosity and smaller pore size.

8. Suggestions for Future Work

The sintering trials in the performed research studies have been conducted in N_2/H_2 (90/10) atmosphere. This represents a typical protective atmosphere used in industrial practice when sintering oxidation sensitive PM alloys, although the amount of H_2 in N_2/H_2 mixes may vary from a few percent up to 10% or higher. The hydrogen reduces Fe oxide layers on the powder surfaces during the heating stage of the sintering process, as demonstrated by the results shown in Paper III and Paper V, which facilitates the sinter neck formation and the carbothermal reduction of more stable oxides at higher temperature. Hence, the H_2 addition in the protective atmosphere plays an important role. However, it is desirable to keep the H_2 content as low as possible due to cost reasons and the fact that H_2 has a decarburizing effect on the PM steel. Consequently, it is important to investigate the influence of H_2 content in N_2/H_2 protective atmospheres on the oxide reduction process during sintering of PM steel prealloyed with Cr and Mn. This issue is already being investigated in an ongoing research program at Chalmers University of Technology, in which studies of the influence of heating rate and sintering time on the oxide reduction process also are being conducted. These studies will generate valuable complementary information to the results and conclusions presented in this thesis.

Another interesting issue recommended for future research work is the effect of CO additions to the protective atmosphere on the oxide reduction process during sintering. The performed research work shows that reduction of stable Cr-Mn oxides in the PM steel compacts occurs through carbothermal reactions, which suggests that CO additions to the sintering atmosphere can give more effective reduction in accordance with reaction (11) in sub-chapter 4.3. Furthermore, using controlled additions of CO to N_2/H_2 atmospheres is a method to control the carbon content of the PM steel in the sintering process, as described in sub-chapter 2.4. Consequently, N_2-H_2-CO mixes might be suitable sintering atmospheres for PM steel grades prealloyed with Cr and Mn both in the aspect of carbon control and for achieving effective oxide reduction.

The performed research studies have also demonstrated that residual oxides after sintering in the investigated PM steel have no obvious detrimental effect on the static mechanical properties of the sintered material. The residual oxide particulate features are small (of micrometer size) in comparison with the size of the largest pores in the PM parts, which is typically >20 μm for part densities up to 7.3 g/cm^3. Hence, the pores are the dominant defects and the oxides do not affect the mechanical performance of the PM steel. Even in PM parts with very high density (7.5 g/cm^3) there are pores larger than 10 μm, which is shown by the results in Paper IV and Paper V. However, these high density parts also contain clusters of residual oxides that are up to a few micrometers in size. Fatigue testing of high density specimens (7.5 g/cm^3) should clarify if such oxide features could have any significant detrimental effect on the mechanical performance of PM steel prealloyed with Cr and Mn.

9. Acknowledgments

First of all I would like to thank my supervisor Professor Lars Nyborg for his support and enthusiastic involvement in my research work. This has been very valuable and his guidance was crucial for the progress and outcome of the work presented in this thesis.

I owe gratitude to many people at Höganäs AB for their contributions to the work. The involvement by Sven Bengtsson and Ola Litström has been essential and I am very thankful for their support. Others that have given important input are Ulf Engström, Eva Jacobsson, Sigurd Berg, Hilmar Vidarsson, Robert Frykholm, Björn Lindqvist, Anders Bergmark and Fredrik Persson. The assistance from Mikael Svensson, Eva Ahlfors, Peter Ohlsson, Jenny Westerlund, Siv Olsson and Laila Könsberg in the experimental work is much appreciated. I am also grateful for the support from the Metallography Department, where especially Pernilla Johansson and Heike Grosser have contributed.

My thanks are also extended to Eduard Hryha and Dimitris Chasoglou at Chalmers University of Technology for a very nice teamwork and for the valuable input given by their research work. Special thanks to Eduard for his assistance in my fractography work.

At Swerea KIMAB, I want to thank Karin Frisk for good and fruitful collaboration regarding thermodynamic calculations and oxide reduction. Hans Söderberg and Sophie Caddéo-Johansson are also acknowledged for well-executed sintering trials.

Höganäs AB is gratefully acknowledged for giving me the opportunity to conduct this industrial PhD project and I am also grateful to the Swedish Research Council for the financial support of the project.

Last but not least, I want to thank my beloved wife Cecilia for keeping me motivated by constantly asking when the work will be finished, and my wonderful boys Elias and Daniel for occupying my spare time with football and tennis activities!

10. References

[1] R. M. German: Powder Metallurgy Science, Second Edition, Metal Powder Industries Federation, 1994.

[2] Metal Powder Industries Federation (MPIF), www.mpif.org, 2011.

[3] C. Lindberg: Advances in Powder Metallurgy & Particulate Materials, 1999, Vol. 2, Part 7, pp. 229-243.

[4] S. Berg: Proc. of PM2000 World Congress, Kyoto, Japan, November 2000, JPMA, Vol. 2, pp. 939-944.

[5] P. Ramakrishnan: Indian Journal of History of Science, 1983, Vol. 18, No. 1, pp. 109-114.

[6] Höganäs Handbook for Sintered Components – 1. Material and powder properties, Höganäs AB, 1997.

[7] U. Engström: Proc. of EuroPM2000, Munich, Germany, October 2000, EPMA, Vol. 1, pp. 123-130.

[8] P. Knutsson, K. Olsson, M. Larsson, M. Dahlberg: Proc. of PM2010 World Congress, Florence, Italy, October 2010, EPMA, Vol. 1.

[9] P. Skoglund, M. Kejzelman, I. Hauer: Advances in Powder Metallurgy & Particulate Materials, 2002, Part 4, pp. 85-95.

[10] R. M. German: Sintering Theory and Practice, John Wiley & Sons, 1996.

[11] Z. A. Munir: Powder Metallurgy, 1981, Vol. 24, pp. 177-180.

[12] P.K. Higgins, Z. A. Munir: Powder Metallurgy International, 1982, Vol. 14, pp. 26-29.

[13] S. Kremel, C. Raab, H. Danninger: Proc. of EuroPM2001, Nice, France, October 2001, EPMA, Vol. 1, pp. 52-57.

[14] W. Schatt, K. P. Wieters: Powder Metallurgy – Processing and Materials, European Powder Metallurgy Association, 1997.

[15] C. Franzo, T. Gómez-Acebo, P. Ortiz, J. A. Calero, F. Castro: Proc. of Euro PM2007, Toulouse, France, October 2007, EPMA, Vol. 3, pp. 169-176.

[16] A. Malas, S. Wiberg, D. Nilsson, S. Berg: Advances in Powder Metallurgy & Particulate Materials, 2008, Vol. 2, Part 5, pp. 41-54.

[17] A. Malas, C. Laumen, S. Wiberg, D. Nilsson, S. Berg: Advances in Powder Metallurgy & Particulate Materials, 2009, Vol. 1, Part 5, pp. 23-32.

[18] Höganäs Handbook for Sintered Components – 3. Design and mechanical properties, Höganäs AB, 1997.

[19] Höganäs Iron and Steel Powders for Sintered Components, Höganäs AB, 2002.

[20] Höganäs Handbook for Sintered Components – 6. Metallography, Höganäs AB, 1997.

[21] R. Frykholm, O. Bergman: Advances in Powder Metallurgy & Particulate Materials, 2005, Vol. 3, Part 10, pp. 211-226.

[22] U. Engström: Advances in Powder Metallurgy & Particulate Materials, 2001, Part 7, pp. 204-215.

[23] U. Engström, A. Klekovkin, S. Berg, B. Edwards, L. Frayman, G. Hinzmann, D. Whitehouse: Advances in Powder Metallurgy & Particulate Materials, 2003, Part 7, pp. 68-79.
[24] U. Engström, D. Milligan, A. Klekovkin: Advances in Powder Metallurgy & Particulate Materials, 2006, Vol. 1, Part 7, pp. 21-32.
[25] K. H. Lindner, C. M. Sonsino: Metal Powder Report, 1994, Vol. 49, No. 5, pp. 30-36.
[26] M. Andersson, M. Larsson: Proc. of PM2010 World Congress, Florence, Italy, October 2010, EPMA.
[27] E. M. Daver, C. J. Trombino: Advances in Powder Metallurgy & Particulate Materials, 2007, Vol. 1, pp. i-ix.
[28] R. M. German: Powder Metallurgy & Particulate Materials Processing, Metal Powder Industries Federation, 2005.
[29] E. Hryha, C. Gierl, L. Nyborg, H. Danninger, E. Dudrova: Applied Surface Science, 2010, Vol. 256, No. 12, pp. 3946-3961.
[30] E. Hryha, L. Nyborg: Proc. of PM2010 World Congress, Florence, Italy, October 2010, EPMA, Vol. 2, pp. 268-275.
[31] L. Nyborg, T. Tunberg, P. X. Wang, I. Olefjord: Proc. of PM ´90 World Conference, London, UK, July 1990, The Institute of Metals, Vol. 3, pp. 199-203.
[32] L. Nyborg, T. Tunberg, P. X. Wang: Metal Powder Report, 1990, Vol. 45, No. 11, pp. 750-754.
[33] T. Tunberg, L. Nyborg: Powder Metallurgy, 1995, Vol. 38, No. 2, pp. 120-130.
[34] L. Nyborg, I. Olefjord: Powder Metallurgy, 1988, Vol. 31, No. 1, pp. 33-44.
[35] H. Karlsson, L. Nyborg, S. Berg, Y. Yu: Proc. of Euro PM2001, Nice, France, October 2001, EPMA, Vol. 1, pp. 22-27.
[36] H. Karlsson, L. Nyborg, S. Berg: Powder Metallurgy, 2005, Vol. 48, pp. 51-58.
[37] D. Chasoglou, E. Hryha, L. Nyborg: Proc. of Euro PM2009, Copenhagen, Denmark, October 2009, EPMA, Vol. 2, pp. 181-186.
[38] D. Chasoglou, E. Hryha, L. Nyborg: Proc. of PM2010 World Congress, Florence, Italy, October 2010, EPMA.
[39] E. Hryha, L. Nyborg, S. Bengtsson: Proc. of Euro PM2009, Copenhagen, Denmark, October 2009, EPMA, Vol. 2, pp. 169-174.
[40] H. J. T. Ellingham: Journal of the Society of Chemical Industry, 1944, Vol. 63, pp. 125-133.
[41] F. D. Richardson, J. H. E. Jeffes: Journal of the Iron and Steel Institute, 1948, Vol. 160, pp. 261-270.
[42] Höganäs Handbook for Sintered Components – 2. Production of sintered components, Höganäs AB, 1997.
[43] J. O. Andersson, T. Helander, L. Höglund, P. F. Shi, B. Sundman: Calphad, 2002, Vol. 26, pp. 273-312.
[44] L. Kjellqvist: Doctoral Thesis in Materials Science, KTH Royal Institute of Technology, Stockholm, Sweden, 2009.
[45] J. Arvidsson, O. Eriksson: Proc. of 1998 Powder Metallurgy World Congress, Granada, Spain, Vol. 2, pp. 253-260.

[46] D. L. Douglass, F. Rizzo-Assuncao: Oxidation of Metals, 1988, Vol. 29, pp. 271-287.
[47] T. Brylewski, M. Nanko, T. Maruyama, K. Przybylski: Solid State Ionics, 2001, Vol. 143, pp.131-150.
[48] T. Horita, K. Yamaji, Y. Xiong, H. Kishimoto, N. Sakai, H. Yokokawa: Solid State Ionics, 2004, Vol. 175, pp.157-163.
[49] A. N. Hansson, M. A. J. Somers: Materials at High Temperatures, 2005, Vol. 22, pp. 179-184.
[50] P. Ortiz, F. Castro: Materials Science Forum, 2003, Vols 426-432, pp. 4337-4342.
[51] F. Castro, P. Ortiz: Proc. of Euro PM2003, Valencia, Spain, October 2003, EPMA, Vol. 1, pp. 261-267.
[52] P. Ortiz, F. Castro: Powder Metallurgy, 2004, Vol. 47, pp. 291-298.
[53] S.-J. Kim, I.-S. Byun, H.-Y. Han, H.-L. Yu, S. H. Lee, J.-G. Choi: Applied Catalysis A, 2002, Vol. 234, pp. 35-44.
[54] H. J. Grabke: Materials Science Forum, 1994, Vol. 154, pp. 69-86.
[55] H. Danninger, C. Gierl, S. Kremel, G. Leitner, K. Jaenicke-Roessler, Y. Yu: Powder Metallurgy Progress, 2002, Vol. 2, pp. 125-140.
[56] S. Kremel, H. Danninger, Y. Yu: Powder Metallurgy Progress, 2002, Vol. 2, pp. 211-221.
[57] E. Hryha, L. Cajkova, E. Dudrova, L. Nyborg: Proc. of Euro PM2008, Mannheim, Germany, October 2008, EPMA, Vol. 1, pp. 109-114.
[58] M. Jaliliziyaeian, C. Gierl, H. Danninger: Advances in Powder Metallurgy & Particulate Materials, 2008, Part 5, pp. 72-78.
[59] C. X. Liu, L. Nyborg, T. Tunberg: Proc. of PRICM-1, 1992, The Minerals, Metals & Materials Society, pp. 303-308.
[60] W. Gruner, S. Stolle, K. Wetzig: International Journal of Refractory Metals & Hard Materials, 2000, Vol. 18, pp. 137-145.
[61] L. M. Berger, S. Stolle, W. Gruner, K. Wetzig: International Journal of Refractory Metals & Hard Materials, 2001, Vol. 19, pp. 109-121.
[62] H. Danninger, C. Xu: Proc. of Euro PM2003, Valencia, Spain, October 2003, EPMA, Vol. 1, pp. 269-274.
[63] J.L. Meijering: Acta Metallurgica, 1955, Vol. 3, pp. 157-162.
[64] J. Takada, S. Yamamoto, S. Kikuchi, M. Adachi: Metallurgical Transactions A, 1986, Vol. 17A, pp. 221-229.
[65] C.N. Satterfield: Heterogeneous catalysis in practice, McGraw-Hill Book Company, 1980.
[66] E.N. Fuller, P.D. Schettler, G.C. Giddings: Industrial & Engineering Chemistry, 1966, Vol. 58, Issue 5, pp. 18-27.
[67] N. Wakao, J.M. Smith: Chemical Engineering Science, 1962, Vol. 17, pp. 825-834.
[68] K.K. Kim, J.M. Smith: AlChE Journal, 1974, Vol. 20, No. 4, pp. 670-678.
[69] F. Thümmler, R. Oberacker: Introduction to Powder Metallurgy, The Institute of Materials, 1993.
[70] M. Dlapka, H. Danninger, C. Gierl, B. Lindqvist: Proc. of Euro PM2009, Copenhagen, Denmark, October 2009, EPMA, Vol. 3, pp. 317-322.

[71] H. Söderberg, K. Frisk: Research Report KIMAB-2009-529, Swerea KIMAB AB, 2009.